Zoological Journal of the Linnean Society, 2020, **XX**, 1–22. With 10 figures.

The braincase, brain and palaeobiology of the basal sauropodomorph dinosaur *Thecodontosaurus antiquus*

ANTONIO BALLELL[1,*], J. LOGAN KING[1], JAMES M. NEENAN[2], EMILY J. RAYFIELD[1] and MICHAEL J. BENTON[1]

[1]*School of Earth Sciences, University of Bristol, Bristol BS8 1RJ, UK*
[2]*Oxford University Museum of Natural History, Parks Road, Oxford OX1 3PW, UK*

Received 27 May 2020; revised 15 October 2020; accepted for publication 26 October 2020

Sauropodomorph dinosaurs underwent drastic changes in their anatomy and ecology throughout their evolution. The Late Triassic *Thecodontosaurus antiquus* occupies a basal position within Sauropodomorpha, being a key taxon for documenting how those morphofunctional transitions occurred. Here, we redescribe the braincase osteology and reconstruct the neuroanatomy of *Thecodontosaurus*, based on computed tomography data. The braincase of *Thecodontosaurus* shares the presence of medial basioccipital components of the basal tubera and a U-shaped basioccipital–parabasisphenoid suture with other basal sauropodomorphs and shows a distinct combination of characters: a straight outline of the braincase floor, an undivided metotic foramen, an unossified gap, large floccular fossae, basipterygoid processes perpendicular to the cultriform process in lateral view and a rhomboid foramen magnum. We reinterpret these braincase features in the light of new discoveries in dinosaur anatomy. Our endocranial reconstruction reveals important aspects of the palaeobiology of *Thecodontosaurus*, supporting a bipedal stance and cursorial habits, with adaptations to retain a steady head and gaze while moving. We also estimate its hearing frequency and range based on endosseous labyrinth morphology. Our study provides new information on the pattern of braincase and endocranial evolution in Sauropodomorpha.

ADDITIONAL KEYWORDS: anatomy – endocast – Europe – labyrinth – Late Triassic – palaeoecology – palaeoneurology – Rhaetian – Sauropodomorpha – sensory organs.

INTRODUCTION

Dinosaurs originated and diversified in the Triassic, splitting into three major clades: Theropoda, Sauropodomorpha and Ornithischia. The first dinosaurs were small bipeds (Carrano, 1999, 2000) with either faunivorous or omnivorous habits (Barrett & Rayfield, 2006; Barrett *et al.*, 2011; Barrett, 2014; Cabreira *et al.*, 2016), but it is not fully understood how these early forms diversified their diets and body sizes to include several herbivorous lineages by the end of the Triassic. One of the earliest members of the Sauropodomorpha is *Thecodontosaurus antiquus* Morris, 1843, the first Triassic dinosaur to be named (Riley & Stutchbury, 1836, 1840) and only the sixth dinosaur ever named in the world. The original material was described by Benton *et al.* (2000), including a detailed account of an exquisite, complete braincase and endocast, and a more complete assemblage of *Thecodontosaurus* fossils has been described recently (Ballell *et al.*, 2020). *Thecodontosaurus* had always been regarded as Carnian in age, although regional geological and palynological evidence now points much more convincingly to a latest Triassic (Rhaetian) age, 205–201 Mya (Whiteside *et al.*, 2016). *Thecodontosaurus* occupies a basal position within Sauropodomorpha as one of the non-massopodan Triassic taxa, more derived than *Bagualosaurus* Pretto, Langer & Schultz, 2018 but more basal than *Efraasia* Galton, 1973 (Gauthier, 1986; Benton *et al.*, 2000; Yates & Kitching, 2003; Upchurch *et al.*, 2007; Otero & Pol, 2013; Langer *et al.*, 2019; McPhee *et al.*, 2020). *Thecodontosaurus* is therefore important in terms of establishing the early evolutionary history of Sauropodomorpha.

Throughout their early evolution, sauropodomorphs underwent drastic morphological and functional modifications that led to shifts in their feeding and

*Corresponding author. E-mail: ab17506@bristol.ac.uk

locomotory styles, linked to a general trend towards increased body size (Sander, 2013). Traditionally, the first dinosaurs were considered to be carnivores (Sereno, 1997; Nesbitt *et al.*, 2010), but recent evidence shows that the plesiomorphic dietary condition of this clade is ambiguous depending on different phylogenetic scenarios, and omnivory is equally possible (Barrett & Rayfield, 2006; Barrett *et al.*, 2011; Barrett, 2014; Cabreira *et al.*, 2016). Nonetheless, early sauropodomorphs transitioned from obligatory or facultative faunivory to herbivory via an intermediate omnivorous state (Barrett, 2014; Button *et al.*, 2016; Cabreira *et al.*, 2016; Müller *et al.*, 2018; Bronzati *et al.*, 2019; Müller & Garcia, 2019). Changes in locomotory mode occurred later in the evolution of the group, and the acquisition of a quadrupedal gait involved a previous phase of facultative quadrupedalism and reversals to bipedalism in some lineages (McPhee *et al.*, 2018). These functional innovations in feeding and locomotion were triggered not only by cranial and postcranial musculoskeletal adaptations, but also by modifications of the brain and sensory organs (Bronzati *et al.*, 2017). As a result, early sauropodomorphs constituted an ecologically diverse assemblage.

Braincase anatomy is a remarkable source of information to infer the palaeobiology of extinct vertebrates because brain and inner ear morphology can be reconstructed from endocasts, but with some limitations (Dutel *et al.*, 2019; Evers *et al.*, 2019). These are primarily that, depending on the taxon and ontogeny of the individual, the surface of the brain can be obscured by a thick dural envelope (dura mater) that covers the entirety of the endocast (Jirak & Janacek, 2017). Even so, the presence, absence and relative sizes of different regions of the endocast can tell us about the sensory systems, balance and posture of extinct animals (Witmer *et al.*, 2003, 2008; Witmer & Ridgely, 2009). Application of up-to-date imaging techniques, such as computed tomography (CT), has greatly increased the knowledge of braincase and endocranial morphology in different dinosaur lineages (e.g. Sampson & Witmer, 2007; Witmer & Ridgely, 2009; Miyashita *et al.*, 2011; Lautenschlager *et al.*, 2012; Knoll *et al.*, 2012; Paulina-Carabajal *et al.*, 2018; King *et al.*, 2020), although this information is limited for early dinosaurs because of the scarcity of well-preserved braincases (Martínez *et al.*, 2012; Bronzati *et al.*, 2017, 2018b; Bronzati & Rauhut, 2017). Consequently, the endocranial anatomy and evolution of early sauropodomorphs is notably understudied, with only a few available models (Bronzati *et al.*, 2017; Neenan *et al.*, 2018). The braincase of *Thecodontosaurus* (YPM 2192) is one of the best preserved among early dinosaurs. In their description, Benton *et al.* (2000) created an endocranial model based on external features of the braincase. However, internal details were not accessible, and the brain reconstruction was somewhat speculative.

Here, we present results from segmented CT data, allowing unprecedented access to the details of the braincase and endocast, including the endosseous labyrinth, not seen before. The new anatomy enables us to determine certain aspects of the sensory systems of *Thecodontosaurus*, hence to resolve some debated issues about its palaeobiology and the early evolution of sauropodomorph dinosaurs.

Institutional abbreviations

BRSMG, Bristol City Museum and Art Gallery, Bristol, UK; YPM, Yale Peabody Museum, New Haven, CT, USA.

MATERIAL AND METHODS

Specimen and sampling

Thecodontosaurus antiquus material comes from the Rhaetian fissure fill localities (Whiteside *et al.*, 2016) of Durdham Down (Benton *et al.*, 2000) and Tytherington (Ballell *et al.*, 2020) in south-western England, UK. One of the Durdham Down specimens, YPM 2192, comprises a braincase (Fig. 1A) associated with six vertebrae, ribs and various limb bones. Under this catalogue number, there are 19 isolated specimens in all, and there is no evidence that they were in any way associated, other than that they probably came from the same locality in Bristol and presumably arrived at YPM as a bundle. The *Thecodontosaurus* specimens found in Victorian times were all collected in the 1830s from quarries in Durdham Down, Clifton, on the north side of the Worrall Road, and they were taken exclusively to the BRSMG, which amassed a large collection (Benton *et al.* 2000; Benton, 2012).

The Yale collection includes another fine specimen, YPM 2195, a nearly complete left forelimb, which was acquired in person by Othniel Marsh, then Professor of Paleontology at Yale University, when he visited the Bristol collections in 1888. Marsh arranged the transfer of this and the other specimens to Yale, partly in exchange for American specimens and monographs (Benton *et al.*, 2000; Benton, 2012), and the remainder were sent from Bristol to New Haven in 1888–1889 by the then Bristol curator Edward Wilson (1848–1898), who viewed them as ‘duplicates’.

Computed tomography scanning and three-dimensional model creation

The braincase was scanned at the High-Resolution X-ray CT Facility, University of Texas, Austin, TX, USA, as part of the DigiMorph program, in 2005. The scanner

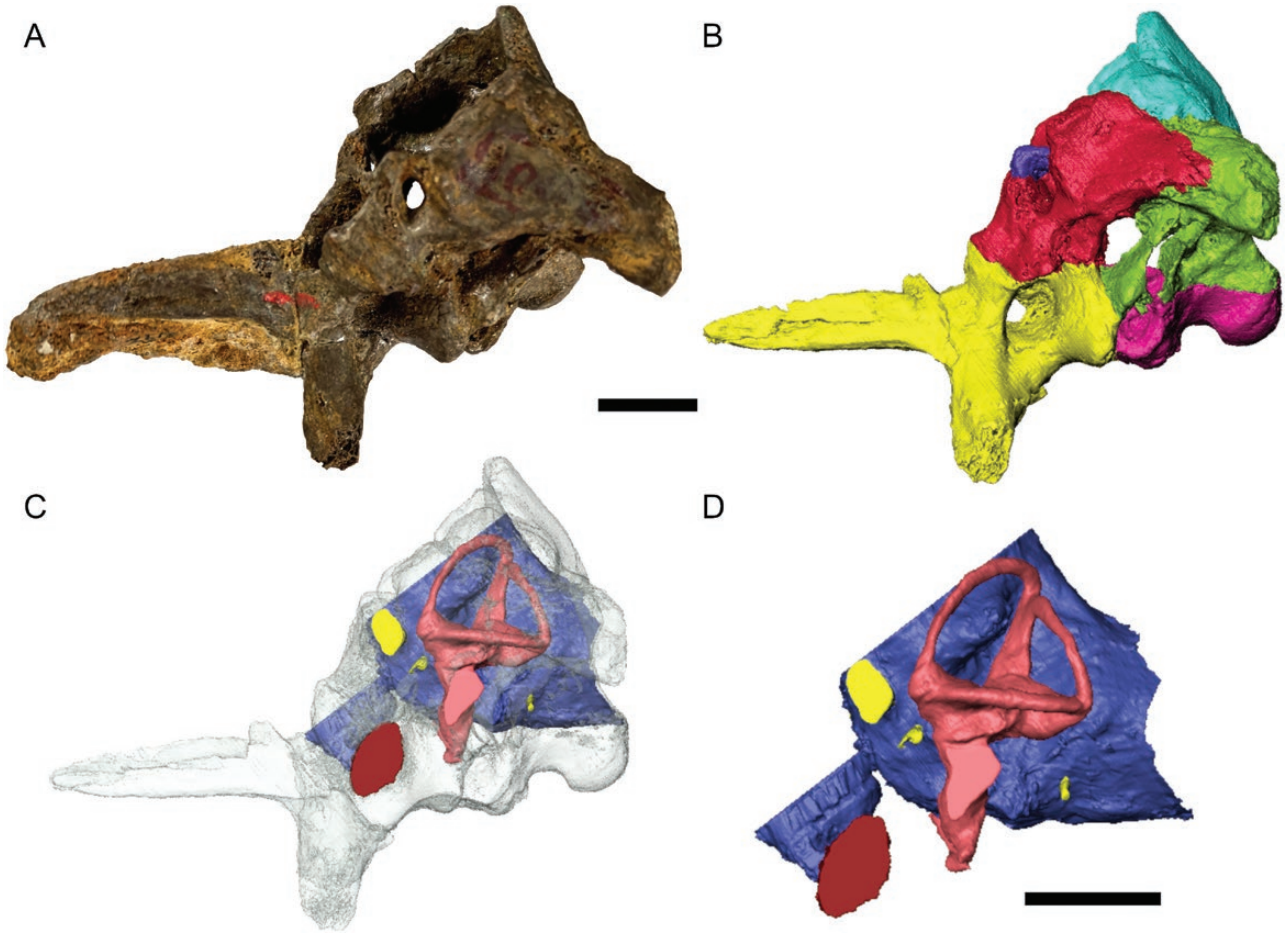

Figure 1. The braincase and endocast of *Thecodontosaurus antiquus*. A, fossil specimen YPM 2192 in left anterolateral view. (courtesy of the Division of Vertebrate Paleontology, YPM 2192, Peabody Museum of Natural History, Yale University, New Haven, Connecticut, USA; peabody.yale.edu) B, segmented three-dimensional (3D) model of the braincase in left lateral view. C, composite of the braincase (transparent) and endocast 3D models. D, segmented 3D model of the endocast in left lateral view, showing brain in blue, labyrinth in pink, nerves in yellow and arteries in red. Scale bars: 1 cm.

was set to 180 kV and 0.133 mA, and the specimen was scanned without offset of the scan axis, using an air wedge and no X-ray filter. The CT images were acquired at a resolution of 1024 × 1025 pixels. Slice thickness corresponded to one line (0.04459 mm), with a source-to-object distance of 131 mm. For each slice, 1400 views were taken, with two samples per view. Image reconstruction was performed with a field of reconstruction of 42.74 mm, an offset of 5000 and a reconstruction scale of 900. The resulting dataset consists of 1480 slices, with voxel size of 0.04174 mm × 0.04174 mm and inter-slice spacing of 0.04459 mm (Supporting Information 1 [CT dataset of the braincase of *Thecodontosaurus antiquus*, YPM 2192, available at the University of Bristol data repository, data.bris, at https://doi.org/10.5523/bris.1hm2mxwxw12ps23gaemx624l8l]).

The CT data were segmented in AVIZO LITE v.9.5 (FEI Visualization Science Group; https://www.fei.com/software/amira-avizo/). The CT scan resolution was high enough to differentiate bone from matrix visually, although insufficient for automatic segmentation. Each bone of the braincase was extracted digitally from the matrix using the paintbrush tool in the *X*, *Y* and *Z* views, and then labelled. The inner cavities of the endocast and the labyrinth were segmented as the endocranium and the inner ear, respectively (Fig. 1B–D, Supporting Information 2 [Surface models (.STL) of the braincase and endocranium of *Thecodontosaurus antiquus*, YPM 2192, available at the University of Bristol data repository, data.bris, at https://doi.org/10.5523/bris.1hm2mxwxw12ps23gaemx624l8l]).

Estimations of hearing frequency

The average and high hearing frequencies (in hertz) of YPM 2192 were calculated accordinging two formulae outlined by Walsh *et al.* (2009):

$$\text{Mean best hearing frequency} = 3311.3x + 4000.8$$

$$\text{Best hearing frequency} = 6104.3x + 6975.2$$

In order to calculate both frequencies, the lengths of the cochlear duct and the basisphenoid are required (Table 1). The basisphenoid was measured (40.28 mm) from the anteriormost extent (approximate location of the parasphenoid–basisphenoid suture) of the basisphenoid to the posteriormost margin of the occipital condyle. The length of the cochlear duct (9.30 mm) was measured from the vestibule to the ventralmost extent of the cochlear duct. A cochlear duct-to-basisphenoid ratio was calculated and logarithmically transformed (represented by x in the above formulae) before being used in the two precalculated formulae for high and mean hearing ranges determined by Walsh *et al.* (2009).

RESULTS

General aspects of the braincase

The specimen YPM 2192 represents a partial braincase described by Benton *et al.* (2000) and assigned to *T. antiquus*. This specimen preserves fairly complete left and right prootics, supraoccipital, left otoccipital, basioccipital and parabasisphenoid, a partial right exoccipital and fragments of the left and right laterosphenoids (Fig. 1).

Basioccipital

The basioccipital is the posteroventral element of the braincase that forms the ventral margin of the foramen magnum and the majority of the occipital condyle (Fig. 2B, D–F). In YPM 2192, this condyle is semicircular in posterior view (Figs 2D, 3E), and tapers slightly anteriorly, ending with a rather straight anterior margin in ventral view (Figs 2B, 3B). The occipital condyle in *Thecodontosaurus* is 1.5 times anteroposteriorly longer than mediolaterally wide, being relatively longer than in other sauropodomorphs, such as *Saturnalia* Langer, Abdala, Richter & Benton 1999 (Bronzati *et al.*, 2018b), *Efraasia* (Bronzati & Rauhut, 2017) and *Adeopapposaurus* Martínez, 2009, in which it is anteroposteriorly compressed. The elongate occipital condyle was considered an apomorphy of *Thecodontosaurus* by Benton *et al.* (2000), although it is also present in *Pantydraco* Galton, Yates & Kermack, 2007 (Galton & Kermack, 2010) and in other taxa, such as *Plateosaurus* von Meyer, 1837 (Prieto-Márquez & Norell, 2011) and *Unaysaurus* Leal *et al.*, 2004 (McPhee *et al.*, 2020).

The dorsal surface of the basioccipital (Fig. 3A) bears a relatively broad neural groove, which runs along the anteroposterior length of the bone and represents the ventral floor of the endocranium. In the anterior third of the basioccipital, where the bone expands laterally, doubling its width, the endocranial floor is split in two by a median ridge, as in *Pantydraco* (Galton & Kermack, 2010) and *Lesothosaurus* Galton, 1978 (Porro *et al.*, 2015). At the level of the posterior end of the median ridge, the paired metotic fissures (Fig. 3A) branch laterally from the endocranial floor. These grooves are anteroposteriorly broad, as seen in *Pantydraco* (Galton & Kermack, 2010). The endocranial floor is bounded laterally by the dorsolaterally facing otoccipital articular surfaces, which form tight basioccipital–otoccipital sutures.

A remarkable feature of the basioccipital is the presence of an unossified gap on the lateral surface of the basioccipital portion of the basal tubera (Figs 2E, 3C), a common feature among basal sauropodomorphs and other groups of archosauriforms that is lost in Sauropoda (Bronzati & Rauhut, 2017). This gap would have been occupied by cartilaginous tissue, as suggested by Benton *et al.* (2000).

On the ventral surface of the bone, the basioccipital neck departs from the anterior end of the occipital condyle to reach the basal tubera (Figs 2B, 3B). The neck is not ventrally prominent, forming a strong dorsally convex lateral outline between the occipital condyle and the basal tubera. The basal tubera are broad, anterolaterally orientated paired ridges with robust medial ends, separated by a shallow sagittal groove. These structures are narrower than those of *Massospondylus* Owen, 1854 (Chapelle & Choiniere, 2018). A deep median notch is present anterior to the basal tubera and anteriorly bounded by the basioccipital–parabasisphenoid suture. In ventral view, this suture presents the typical anteriorly

Table 1. Measurements of endosseous labyrinth structures

Structure	Length (mm)
Anterior semicircular canal	15.4
Posterior semicircular canal	11.5
Lateral semicircular canal	6.0
Crus commune	7.3
Endosseous cochlear duct	9.3

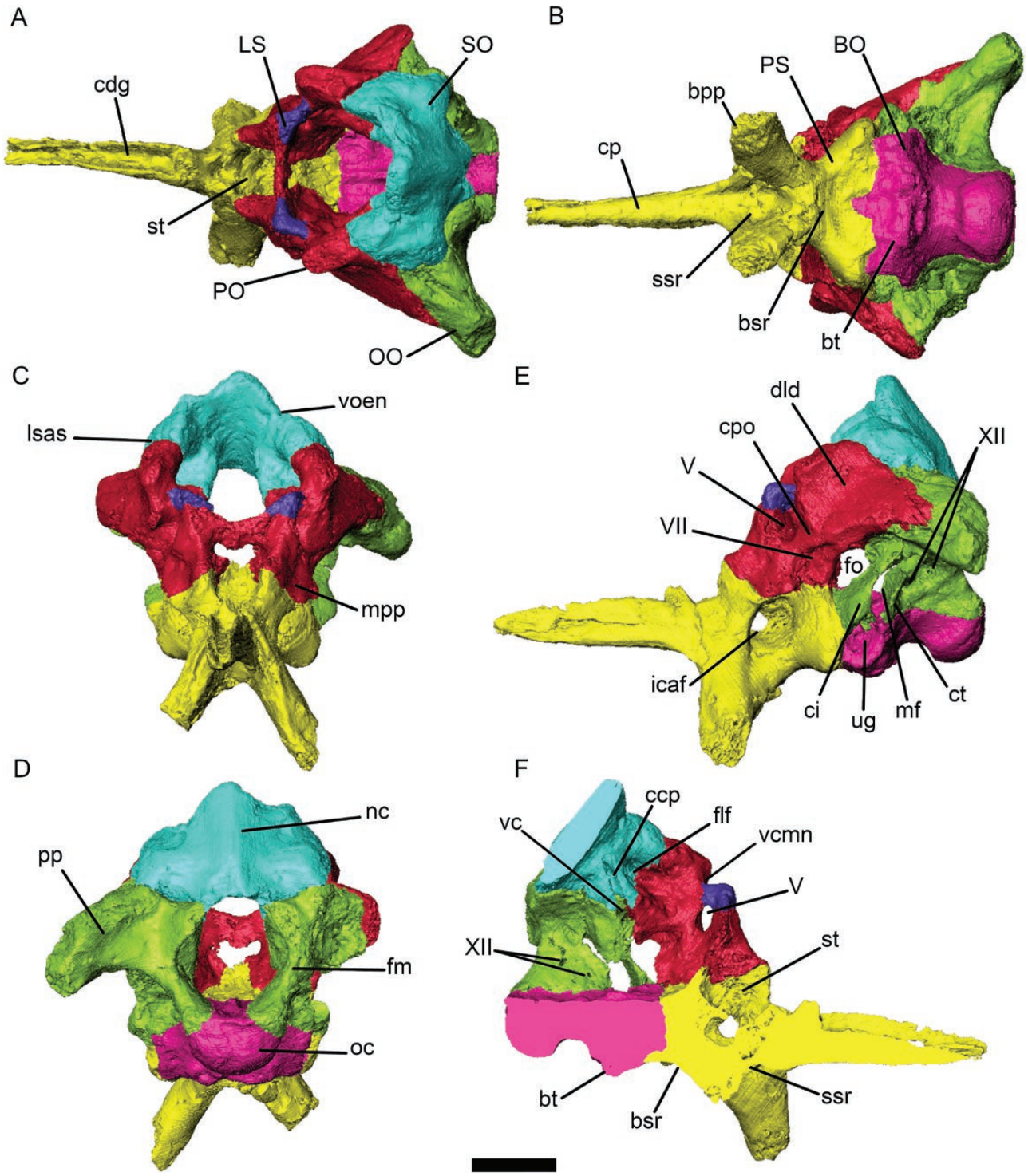

Figure 2. Model of the braincase of *Thecodontosaurus antiquus*, specimen YPM 2192, in dorsal (A), ventral (B), anterior (C), posterior (D), left lateral (E) and left internal (F) views. Abbreviations: BO, basioccipital; bpp, basipterygoid process; bsr, basisphenoid recess; bt, basal tubera; ccp, crus commune passage; cdg, dorsal groove of cultriform process; ci, crista interfenestralis; cp, cultriform process; cpo, crista prootica; ct, crista tuberalis; dld, dorsolateral depression of prootic; flf, floccular fossa; fm, foramen magnum; fo, foramen ovale; icaf, internal carotid foramina; LS, laterosphenoid; lsas, laterosphenoid articular surface; mf, metotic foramen; mpp, musculus protactor pterygoideus attachment site; nc, nuchal crest; oc, occipital condyle; OO, otoccipital; PO, prootic; pp, paraoccipital process; PS, parabasisphenoid; SO, supraoccipital;

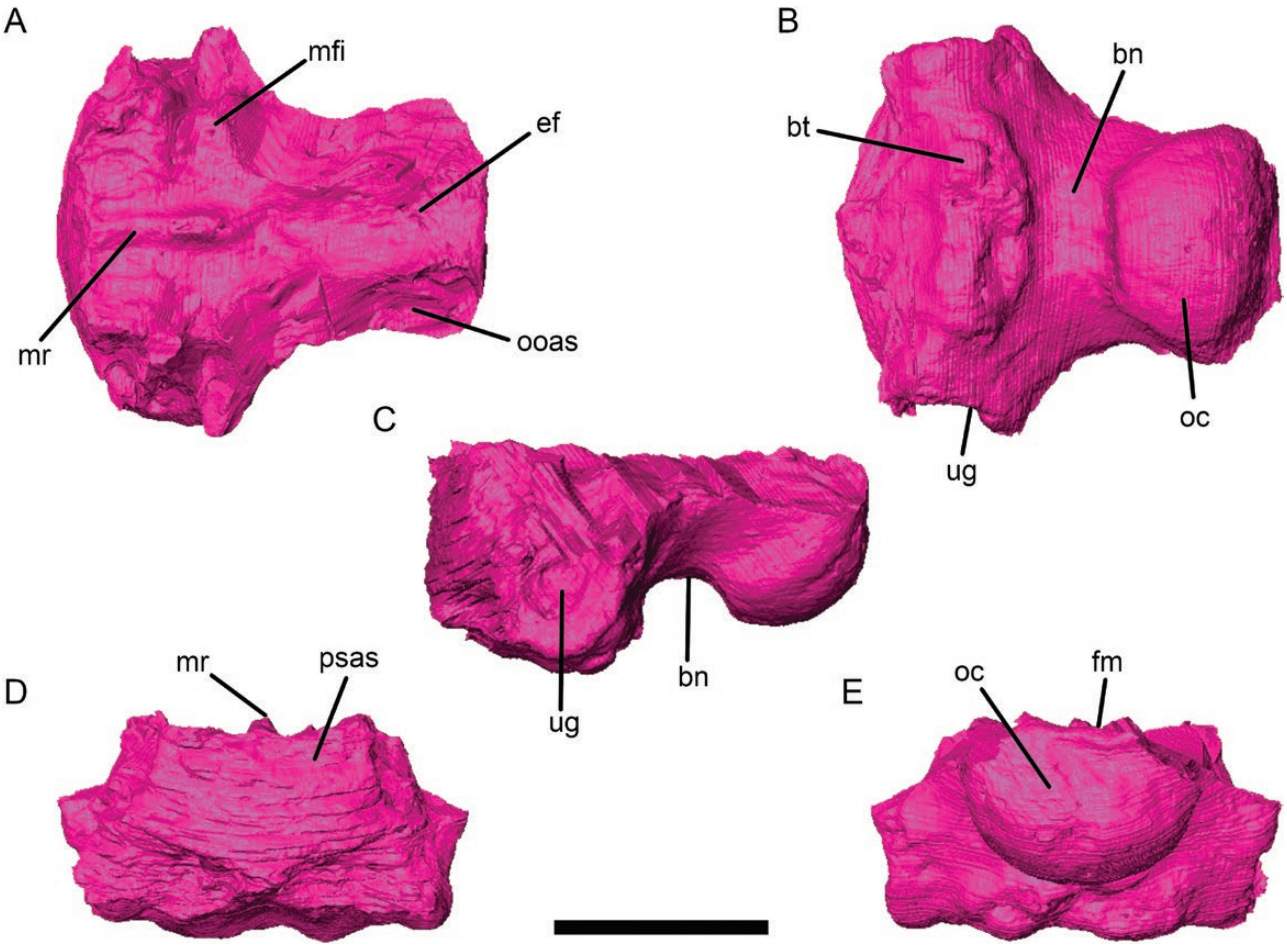

Figure 3. Model of the basioccipital of *Thecodontosaurus antiquus*, specimen YPM 2192, in dorsal (A), ventral (B), left lateral (C), anterior (D) and posterior (E) views. Abbreviations: bn, basioccipital neck; bt, basal tubera; ef, endocranial floor; fm, foramen magnum; mfi, metotic fissure; mr, median ridge; oc, occipital condyle; ooas, otoccipital articular surface; psas, parabasisphenoid articular surface; ug, unossified gap. Scale bar: 1 cm.

concave, U-shaped morphology seen in non-sauropodan sauropodomorphs, such as *Efraasia* (Bronzati & Rauhut, 2017), *Saturnalia* (Bronzati *et al.*, 2018b) and *Unaysaurus* (McPhee *et al.*, 2020).

Parabasisphenoid

The parabasisphenoid is formed by the basisphenoid and the parasphenoid, which are completely co-ossified, the usual condition among archosauriforms (Bittencourt *et al.*, 2015). This bone represents the anterior part of the endocranial floor. The parabasisphenoid reaches its maximal width at the basioccipital suture and tapers sharply anterior to this point. The posterodorsal surface of the bone forms the prootic articular surface, the anterior portion of which is located at the preotic pendant (Figs 2E, 4D). The parabasisphenoid forms the anteroventral portion of this structure, and it exhibits an anterodorsal concave surface that represents the origin of musculus protactor pterygoideus, as suggested by Benton *et al.* (2000), which can be also identified at the same position in *Saturnalia* (Bronzati *et al.*, 2018b) and *Adeopapposaurus* (Martínez, 2009).

The sella turcica (Figs 2A, F, 4A) is a large and deep depression on the dorsal surface of the parabasisphenoid, which contained the pituitary. In dorsal view it is ellipsoid, with an anteroposterior long axis, and has a greater relative volume than in *Saturnalia* (Bronzati *et al.*, 2018b) and *Lesothosaurus* (Porro *et al.*, 2015) and similar to *Massospondylus*

ssr, subsellar recess; st, sella turcica; ug, unossified gap; V, trigeminal nerve (cranial nerve V) foramen; vc, vestibular chamber; vcmn, vena cerebralis media notch; VII, facial nerve (cranial nerve VII) foramen; voen, vena occipitalis externa notch; XII, hypoglossal nerve (cranial nerve XII) foramina. Scale bar: 1 cm.

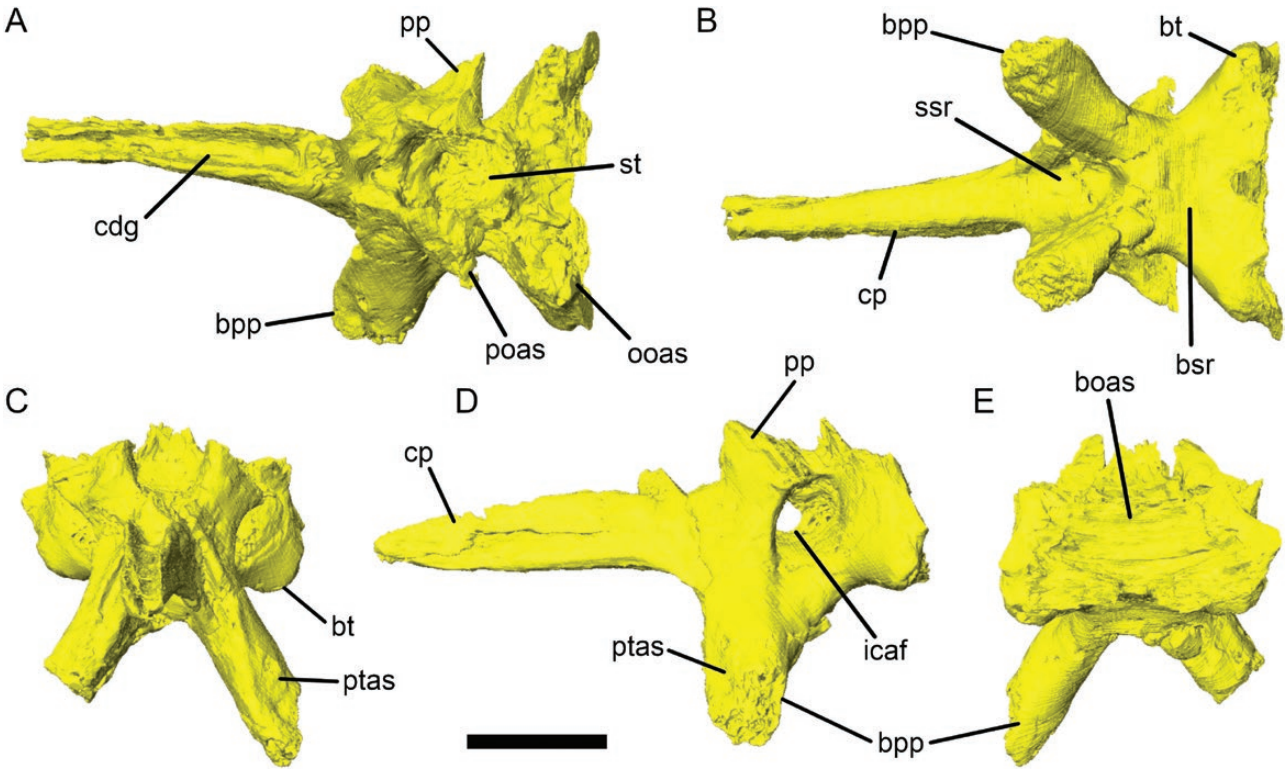

Figure 4. Model of the parabasisphenoid of *Thecodontosaurus antiquus*, specimen YPM 2192, in dorsal (A), ventral (B), anterior (C), left lateral (D) and posterior (E) views. Abbreviations: boas, basioccipital articular surface; bpp, basipterygoid process; bsr, basisphenoid recess; bt, basal tubera; cdg, dorsal groove of cultriform process; cp, cultriform process; icaf, internal carotid foramina; ooas, otoccipital articular surface; poas, prootic articular surface; pp, preotic pendant; ptas, pterygoid articular surface; ssr, subsellar recess; st, sella turcica. Scale bar: 1 cm.

(Chapelle & Choiniere, 2018) and *Adeopapposaurus* (Martínez, 2009). The anterior half of the sella turcica is deeper than the posterior half, with the former presenting a ventrolateral surface perforated by two large internal carotid foramina (Figs 2E, F, 4D). Benton *et al.* (2000) reconstructed the passage for the internal carotid arteries as a single opening of the vidian canal, located anterior to the sella turcica. Here, we interpret this structure as a shallow dorsal fossa at the posterior end of the cultriform process, with no continuation as a canal. The posterolateral surface of the parabasisphenoid presents a large opening, corresponding to the external foramina for the internal carotid artery, which connects the sella turcica with the exterior of the braincase via a short and remarkably wide canal that has a mainly mediolateral orientation.

The parabasisphenoid basal tubera (Figs 2B, 4B–E) project ventrolaterally and are more acute than those seen in other basal sauropodomorphs (Martínez, 2009; Chapelle & Choiniere, 2018; Bronzati *et al.*, 2018b). The contribution of the parabasisphenoid to the lateral portion of the basal tubera is relatively minor in YPM 2192 compared with the condition seen in *Saturnalia* (Bronzati *et al.*, 2018b) and *Massospondylus* (Chapelle & Choiniere, 2018), because of the lateral unossified gaps. The ventral surface between the basal tubera is occupied by a shallow and laterally wide basisphenoid recess (Figs 2B, 4B), anteriorly bounded by a mediolaterally orientated ridge located between the basipterygoid processes. These processes are finger-like, exhibiting slight mediolateral compression and with a total length of 13 mm (Fig. 4A–E). The ventral end of the right basipterygoid process is missing, but its left counterpart presents an anterolateral depression that marks the contact with the pterygoid (Fig. 4C, D). In lateral view, the basipterygoid processes form an angle of 90° with the cultriform process, similar to *Adeopapposaurus* (Martínez, 2009) and unlike *Saturnalia* (Bronzati *et al.*, 2018b), *Pantydraco* (Galton & Kermack, 2010) and *Efraasia* (Bronzati & Rauhut, 2017), where they form an acute angle. This character nonetheless seems to be affected by ontogeny, as seen in ontogenetic series of *Massospondylus carinatus* Owen, 1854 (Chapelle & Choiniere, 2018). The subsellar recess (Figs 2B, F, 4B), a ventral fossa located anterior to the base of

the basipterygoid processes, is remarkably deep, as seen in *Efraasia* (Bronzati & Rauhut, 2017). The subsellar recess is not anteriorly delimited by the ventral laminae that extend from the base of the basipterygoid processes, unlike in plateosaurids and *Melanorosaurus* (Yates, 2007; Prieto-Márquez & Norell, 2011; Bronzati & Rauhut, 2017; McPhee *et al.*, 2020).

The cultriform process (Figs 2, 4) is the anteriormost feature of the parabasisphenoid and represents ~60% of the length of the bone. It is tilted slightly towards the right side compared with the rest of the braincase owing to taphonomic deformation. The cultriform process bears a deep dorsal groove (Fig. 2A, 4A) along its whole length except for the posterior base. The ventral outline of this process is slightly concave, intermediate between the more pronounced curvature seen in *Massospondylus* (Chapelle & Choiniere, 2018) and the straight ventral margins present in *Saturnalia* (Bronzati *et al.*, 2018b) and *Adeopapposaurus* (Martínez, 2009). The cultriform process in YPM 2192 is shorter and dorsoventrally deeper than in these three sauropodomorph taxa (Martínez, 2009; Chapelle & Choiniere, 2018; Bronzati *et al.*, 2018b). The cultriform process, the base of the basipterygoid processes and the occipital condyle are aligned, forming a straight ventral margin of the braincase in lateral view, as seen in *Pantydraco* (Galton & Kermack, 2010), *Efraasia* (Bronzati & Rauhut, 2017) and *Adeopapposaurus* (Martínez, 2009). This contrasts with the dorsally offset basioccipital condyle (the 'stepped' braincase morphology) of *Saturnalia* (Bronzati *et al.*, 2018b), *Plateosaurus* (Prieto-Márquez & Norell, 2011), *Coloradisaurus* Lambert, 1983 (Apaldetti *et al.*, 2014) and *Lufengosaurus* Young, 1941 (Barrett *et al.*, 2005).

Laterosphenoid

The laterosphenoids are not preserved except for a reduced portion that contacts the clinoid process of the prootics, forming the anterodorsal margin of the cranial nerve (CN) V (trigeminal) foramen (Fig. 2). This reconstruction contradicts the interpretation of the prootic being the only bone contributing to the trigeminal foramen, expounded by Benton *et al.* (2000).

Prootic

The paired prootics form the dorsolateral walls of the braincase. They contact the supraoccipital dorsomedially, the otoccipital posteromedially, the parabasisphenoid ventrally and the laterosphenoid anterodorsally (Fig. 2). The prootic contains the anterior portion of the endosseous labyrinth, which is visible on the posterior surface of the bone (Fig. 5B), occupied by the otoccipital articular surface. A large opening on this surface shows the anterior portion of the vestibular chamber, which continues posteriorly with a groove (Fig. 5B) that marks the passage of the lateral semicircular canal (LSC). The dorsomedial surface of the prootic bears the supraoccipital articular surface, where the foramen for the passage of the anterior semicircular canal (ASC) is present, entering the bone vertically (Fig. 5E, F). The prootic presents a dorsoventrally elongated depression on its medial surface, penetrating between the supraoccipital and otoccipital articular surfaces and located dorsal to the trigeminal foramen. This deep depression is the floccular fossa (Figs 2F, 5E), which housed the well-developed floccular lobe of the cerebellum.

The posterolateral ramus of the prootic anteriorly overlaps the proximal part of the paroccipital process and is distally acute in the more complete left prootic (Fig. 5D, E). Anterior to it, the prootic shows a marked dorsolateral depression (Figs 2E, 5C, D), interpreted as the dorsal tympanic recess (Witmer, 1997; Rauhut, 2004; Bronzati & Rauhut, 2017; Bronzati *et al.*, 2018b) or an attachment site for the jaw adductor musculature, probably a branch of the musculus adductor mandibulae externus group (Martínez *et al.*, 2012; Porro *et al.*, 2015).

A robust crista prootica (Figs 2E, 5D) connects the dorsolateral depression with the musculus protactor pterygoideus attachment site and separates the CN V notch and the CN VII foramen. The trigeminal foramen is a large, oval opening formed mainly by the prootic. A deep lateral groove emerges posteriorly from this foramen, possibly representing the path for the mandibular branch (CN V_3) of the trigeminal nerve, as suggested by Chapelle & Choiniere (2018) for *Massospondylus* based on CN reconstructions in extinct crocodylomorphs (Holliday & Witmer, 2009). Dorsal to the trigeminal foramen and ventral to the laterosphenoid articular surface, a groove that extends from the interior to the exterior of the braincase marks the passage for the lateral exit of the vena cerebralis media (Figs 2F, 5E), as interpreted by Benton *et al.* (2000) and seen in *Efraasia* (Bronzati & Rauhut, 2017). The facial nerve foramen (Figs 2E, 5C–F) is located posteroventral to the trigeminal foramen, the usual position in basal sauropodomorphs (Martínez, 2009; Galton & Kermack, 2010; Bronzati & Rauhut, 2017; Chapelle & Choiniere, 2018; Bronzati *et al.*, 2018b), and has a smaller diameter than that of CN V. Anteriorly delimited by the crista prootica, it is posteriorly separated from the fenestra ovalis (Fig. 2E) by a second ridge (Fig. 5D). The passage for the facial nerve has a posterolateral course, unlike the trigeminal nerve, which exits the braincase with a more lateral orientation.

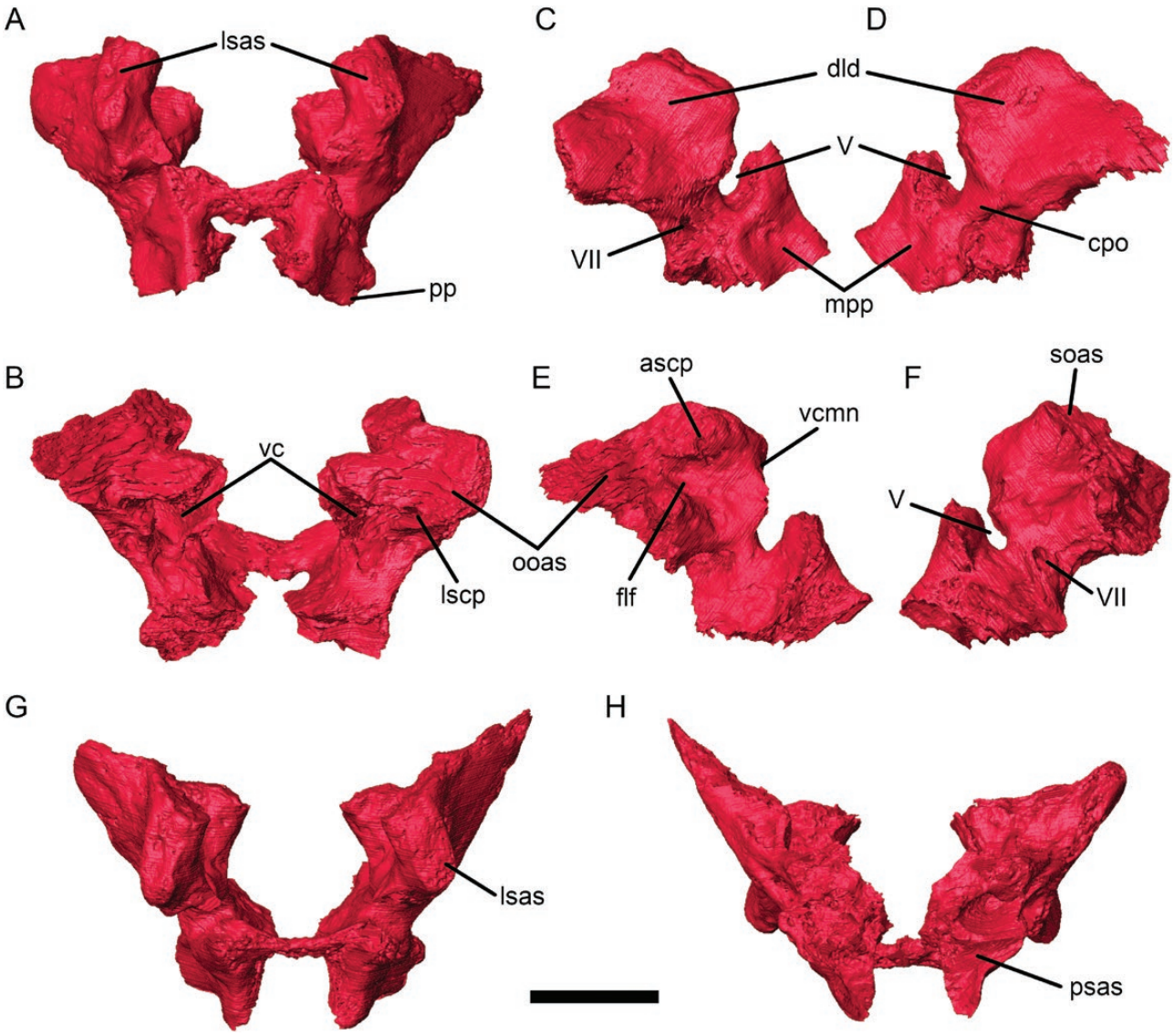

Figure 5. Model of the prootics of *Thecodontosaurus antiquus*, specimen YPM 2192, in anterior (A), posterior (B), right lateral (C), left lateral (D), left medial (E), right medial (F), dorsal (G) and ventral (H) views. Abbreviations: ascp, anterior semicircular canal passage; cpo, crista prootica; dld, dorsolateral depression of prootic; flf, floccular fossa; lsas, laterosphenoid articular surface; lscp, lateral semicircular canal passage; mpp, musculus protactor pterygoideus attachment site; ooas, otoccipital articular surface; pp, preotic pendant; psas, parabasisphenoid articular surface; soas, supraoccipital articular surface; V, trigeminal nerve (cranial nerve V) foramen; vc, vestibular chamber; vcmn, vena cerebralis media notch; VII, facial nerve (cranial nerve VII) foramen. Scale bar: 1 cm.

OTOCCIPITAL

The paired otoccipitals result from the fusion of exoccipitals and opisthotics, the general condition in archosaurs (Sampson & Witmer, 2007), and they constitute the posterodorsal braincase walls (Fig. 2). Given that the right otoccipital is partly damaged, the description is based on the more complete left otoccipital. The otoccipital presents a posterodorsomedial central body, from which three rami project: a pyramidal projection (*sensu* Bronzati & Rauhut, 2017) ventrally, the paroccipital process posterolaterally and the crista interfenestralis (= metotic crest) anteroventrally (Fig. 6E, F).

The pyramidal projection of the otoccipital tapers dorsally and contacts the basioccipital ventrally, with a posteroventral projection forming the dorsolateral portion of the occipital condyle (Figs 2D, 6E, F). The posteromedial portion of the pyramidal projection forms the lateral margin of the foramen magnum

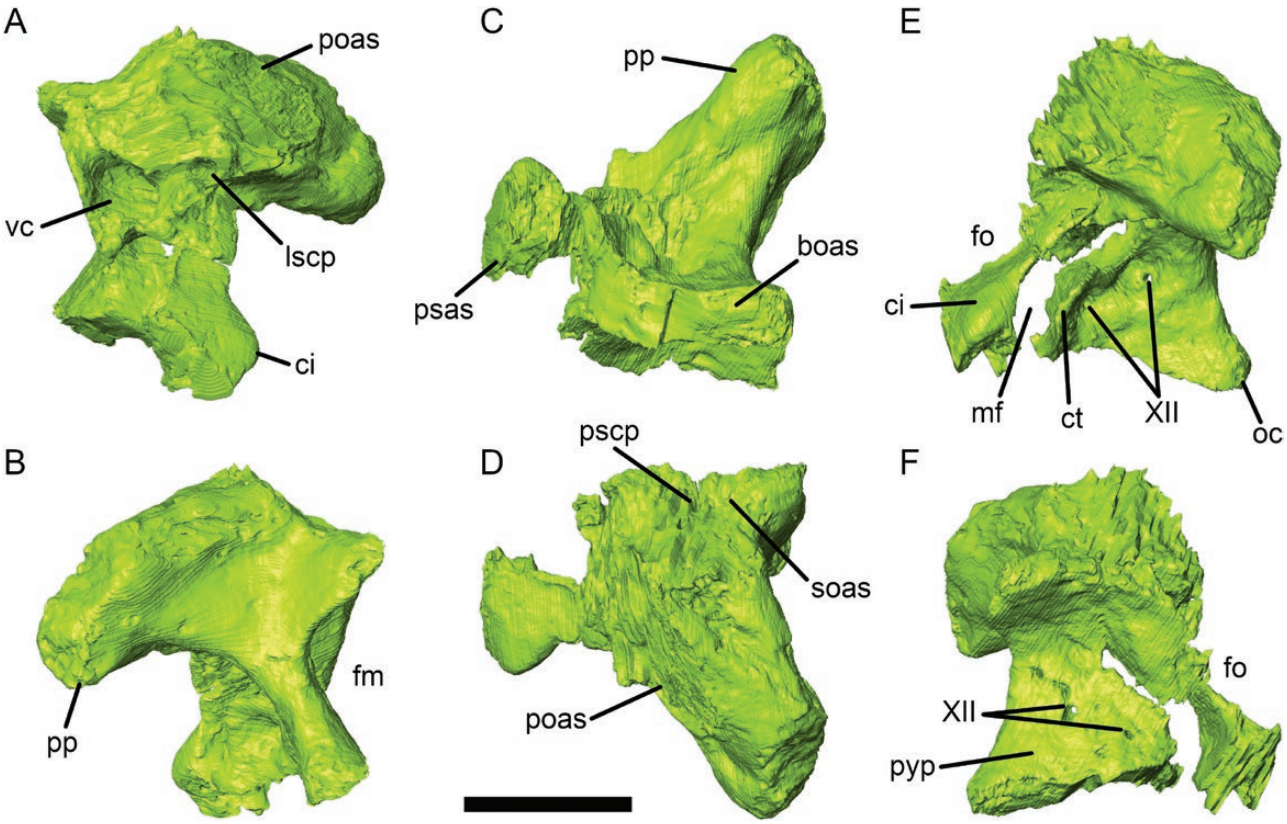

Figure 6. Model of the left otoccipital of *Thecodontosaurus antiquus*, specimen YPM 2192, in anterior (A), posterior (B), ventral (C), dorsal (D), lateral (E) and medial (F) views. Abbreviations: boas, basioccipital articular surface; ci, crista interfenestralis; ct, crista tuberalis; fm, foramen magnum; fo, foramen ovale; lscp, lateral semicircular canal passage; mf, metotic foramen; oc, occipital condyle; poas, prootic articular surface; pp, paraoccipital process; psas, parabasisphenoid articular surface; pscp, posterior semicircular canal passage; pyp, pyramidal projection; soas, supraoccipital articular surface; vc, vestibular chamber; XII, hypoglossal nerve (cranial nerve XII) foramina. Scale bar: 1 cm.

(Figs 2D, 6B), the outline of which is an obtuse angle, contributing to the dorsoventrally elongated rhomboid shape of the foramen magnum. Adeopapposaurus also shows a rhomboid foramen magnum, although dorsoventrally short (Martínez, 2009), whereas this opening is subcircular in *Saturnalia* (Bronzati *et al.*, 2018b) and dorsoventrally higher in *Massospondylus* (Chapelle & Choiniere, 2018). The main body of the pyramidal projection bears two small foramina for the hypoglossal nerve (Fig. 6E, F). The first hypoglossal foramen is anteroventrally placed, close to the metotic fissure, and the second foramen has a central position on the pyramidal projection, located posterodorsally to the first foramen within a deep, oval fossa. The anterior margin of the pyramidal projection is an anterodorsally facing, wide, flat surface, which presents a pronounced lateral ridge, the crista tuberalis (Fig. 6E), which posteriorly bounds the metotic fissure, as seen in *Plateosaurus* (Prieto-Márquez & Norell, 2011).

Both paroccipital processes lack their distal ends, although the left element is more complete. These processes have a posterolateral orientation in YPM 2192, as seen in *Pantydraco* (Galton & Kermack, 2010) and *Adeopapposaurus* (Martínez, 2009), but unlike the more posteriorly directed processes of *Plateosaurus* (Prieto-Márquez & Norell, 2011) and *Massospondylus* (Chapelle & Choiniere, 2018). A deep depression is present on the posterodorsal surface of the otoccipital, between the base of the paroccipital process and the foramen magnum (Fig. 6B), as in other sauropodomorph taxa, such as *Efraasia* (Bronzati & Rauhut, 2017). The anterior surface of the paroccipital process is marked by the prootic articular surface, placed at the base of the process (Fig. 6A, D).

The third ramus of the otoccipital is the anteroventrally orientated crista interfenestralis (Figs 2E, 6E), which separates the fenestra ovalis from the metotic fissure (the foramen lacerum posterior of Benton *et al.*, 2000). The crista interfenestralis is anteroposteriorly flat and mediolaterally broad, with a conical lateroventral projection at its ventral end. Ventrally, the crista interfenestralis contacts the posterolateral corner

of the dorsal surface of the parabasisphenoid. The anteroventrally directed metotic fissure is an anterodorsally narrow opening, which serves as the exit for CNs IX–XI. This opening is usually subdivided in non-sauropodan sauropodomorphs (Bronzati & Rauhut, 2017), although no evidence for more than one foramen is present in YPM 2192, coincident with the interpretation of Benton *et al.* (2000). This condition is also seen in *Plateosaurus* (Prieto-Márquez & Norell, 2011) and *Massospondylus* (Chapelle & Choiniere, 2018) and a *Thecodontosaurus* otoccipital from Tytherington (Ballell *et al.*, 2020). The fenestra ovalis (Figs 2E, 6E, F) is anteriorly delimited by the prootic and posteriorly by the otoccipital. It is oval in shape, with an anteroventral long axis. The fenestra ovalis is dorsoventrally shorter but anteroposteriorly wider than the metotic fissure. It connected the inner ear with the tympanic membrane via the stapes.

The otoccipital is one of the three bones that form the otic capsule, containing the posterior half of the vestibule. This is evident on the anterodorsomedial portion of the bone, where a wide opening on the prootic articular surface shows the interior of the vestibular chamber (Figs 2F, 6A). A groove emerging from the posterodorsal portion of this cavity and a dorsal foramen within the supraoccipital articular surface (Fig. 6D) mark the passage for the posterior semicircular canal (PSC). The circular foramen for the LSC is present at the ventral apex of the prootic articular surface (Fig. 6A), lateral to the otoccipital vestibular cavity.

Supraoccipital

The supraoccipital forms the posterodorsal roof of the endocast and the dorsal margin of the foramen magnum (Fig. 2). In dorsal view, the bone presents a median region with a pronounced sagittal crest, the nuchal crest (Figs 2A, D, 7D), more evident than in *Panphagia* Martínez & Alcober, 2009 (Martínez *et al.*, 2012) and *Massospondylus* (Chapelle & Choiniere, 2018). The anterior margin of the median region of the supraoccipital is laterally bounded by two notches for the posterior exit of the vena cerebralis media, also named 'vena occipitalis externa' (Figs 2C, 7A), which are shallower in YPM 2192 than in *Panphagia* Martínez & Alcober, 2009 (Martínez *et al.*, 2012) and *Massospondylus* (Chapelle & Choiniere, 2018). In *Coloradisaurus*, these notches are completely enclosed by the supraoccipital and become foramina (Apaldetti *et al.*, 2014).

In anterior view, the supraoccipital is shaped like an arch, with lateral walls descending ventrally from the median region to contact the otoccipitals and prootics.

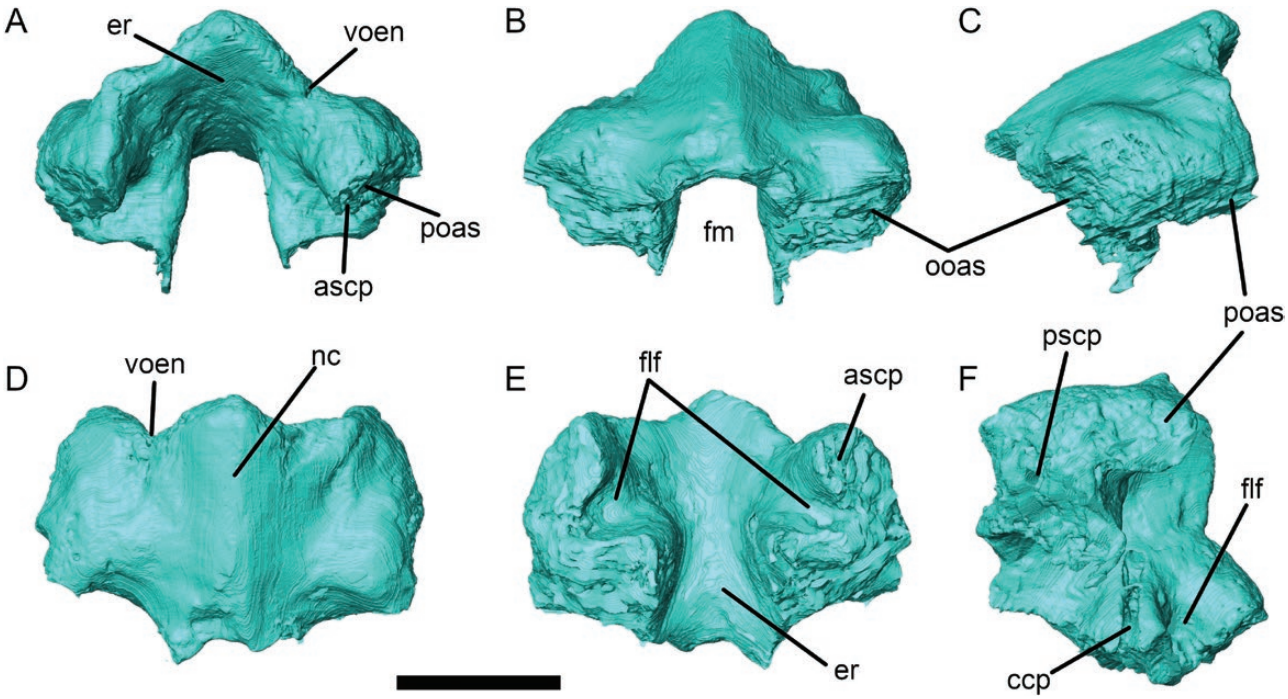

Figure 7. Model of the supraoccipital of *Thecodontosaurus antiquus*, specimen YPM 2192, in anterior (A), posterior (B), right lateral (C), dorsal (D), ventral (E) and right ventrolateral (F) views. Abbreviations: ascp, anterior semicircular canal passage; boas, basioccipital articular surface; ccp, crus commune passage; er, endocranial roof; flf, floccular fossa; fm, foramen magnum; nc, nuchal crest; ooas, otoccipital articular surface; poas, prootic articular surface; pscp, posterior semicircular canal passage; soas, supraoccipital articular surface; voen, vena occipitalis externa notch. Scale bar: 1 cm.

The lateral walls are wider posteriorly (Fig 7E), at the otoccipital articular surface, which means that the roof of the endocranial cavity widens anteriorly, marking the transition from medulla oblongata to cerebellum. At this transition point, the lateral walls present an anteroventrally orientated medial depression, which is continuous with the medial fossae of the prootics, representing the floccular fossae (Figs 2F, 7E, F).

The supraoccipital is the third element forming the labyrinth, particularly enclosing the passages for the ASC and PSC. The wider of these passages is the canal for the crus commune, which opens medioventrally at the junction between the otoccipital and prootic articular surfaces, entering the vestibular chamber located in these two bones (Fig. 2F). The crus commune canal has a dorsomedial orientation and is visible on the medial surface of the supraoccipital lateral walls (Fig. 7F) owing to preservation. At its dorsal end, the crus commune branches off, with the PSC passage continuing posterolaterally to open on the otoccipital articular surface (Fig. 7F), and the ASC passage extending anterolaterally to reach the anteromedial corner of the prootic articular surface (Fig. 7A, E).

CRANIAL ENDOCAST

A partial endocast representing the hindbrain of YPM 2192 was digitally reconstructed (Fig. 8). The endocast comprises the cerebellum, flocculi, the posteriormost portion of the pituitary, medulla oblongata, internal carotid arteries and assorted cranial nerves. The surface of the endocast is smooth and featureless except for the above listed anatomy. Much like other sauropodomorphs, there are no traces of vascularization along the surface of the endocast, indicating that the dura mater was thick enough to obscure the surface anatomy of the brain (Sereno *et al.*, 2007).

Located posterolaterally on the cerebellum are large floccular lobes (Fig. 8A–C, E). The flocculi of YPM 2192 are qualitatively more like *Saturnalia* than like *Plateosaurus* and provide further evidence of when the reduction of sauropodomorph floccular lobes began. These lobes are angled posteriorly at 150° and are one of the most noticeable features of the endocast owing to their size. The flocculi have a triangular cross-section and fill most of the vestibular portion of the endosseous labyrinths (Figs 8, 9). Much like other basal sauropodomorphs (Galton, 1985; Gow,

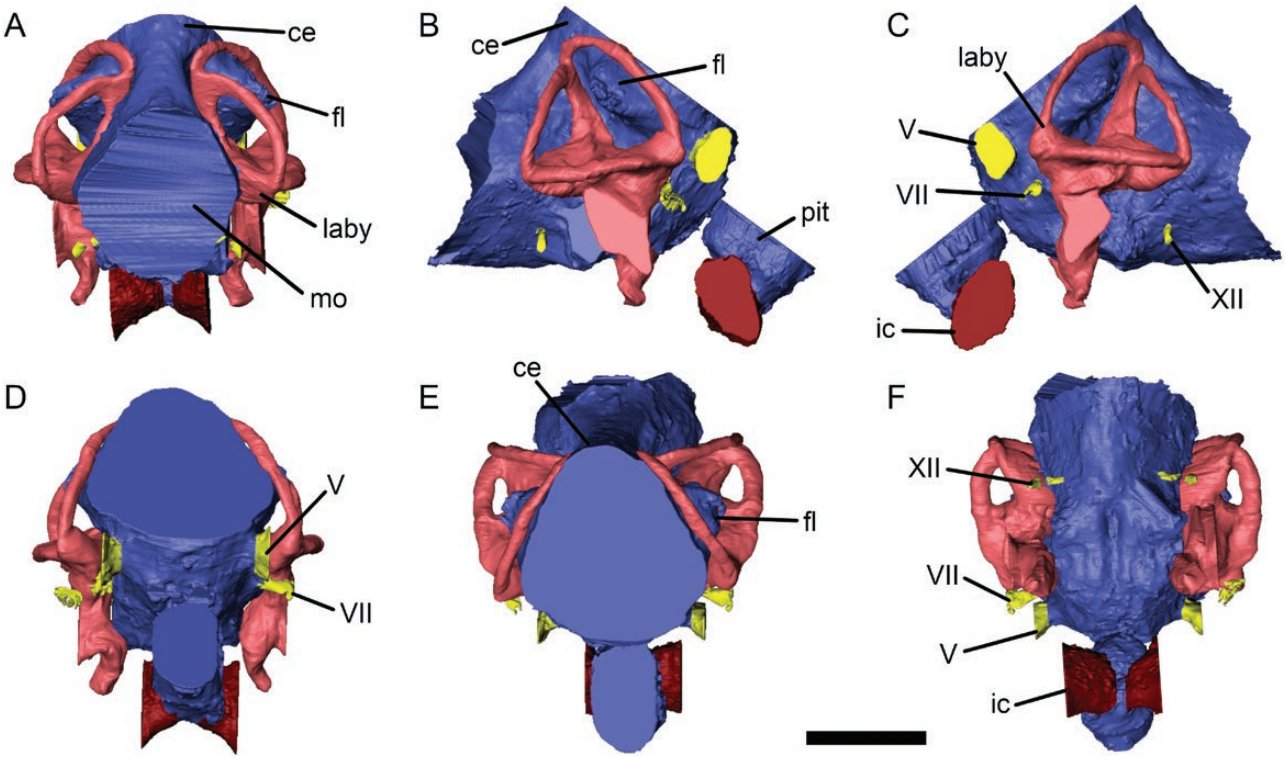

Figure 8. Model of the endocast of *Thecodontosaurus antiquus*, specimen YPM 2192, in posterior (A), right lateral (B), left lateral (C), anterior (D), dorsal (E) and ventral (F) views. Abbreviations: ce, cerebellum; fl, floccular lobe; ic, internal carotid artery; laby, endosseous labyrinth; mo, medulla oblongata; pit, pituitary; V, trigeminal nerve (cranial nerve V); VII, facial nerve (cranial nerve VII); XII, hypoglossal nerve (cranial nerve XII). Scale bar: 1 cm.

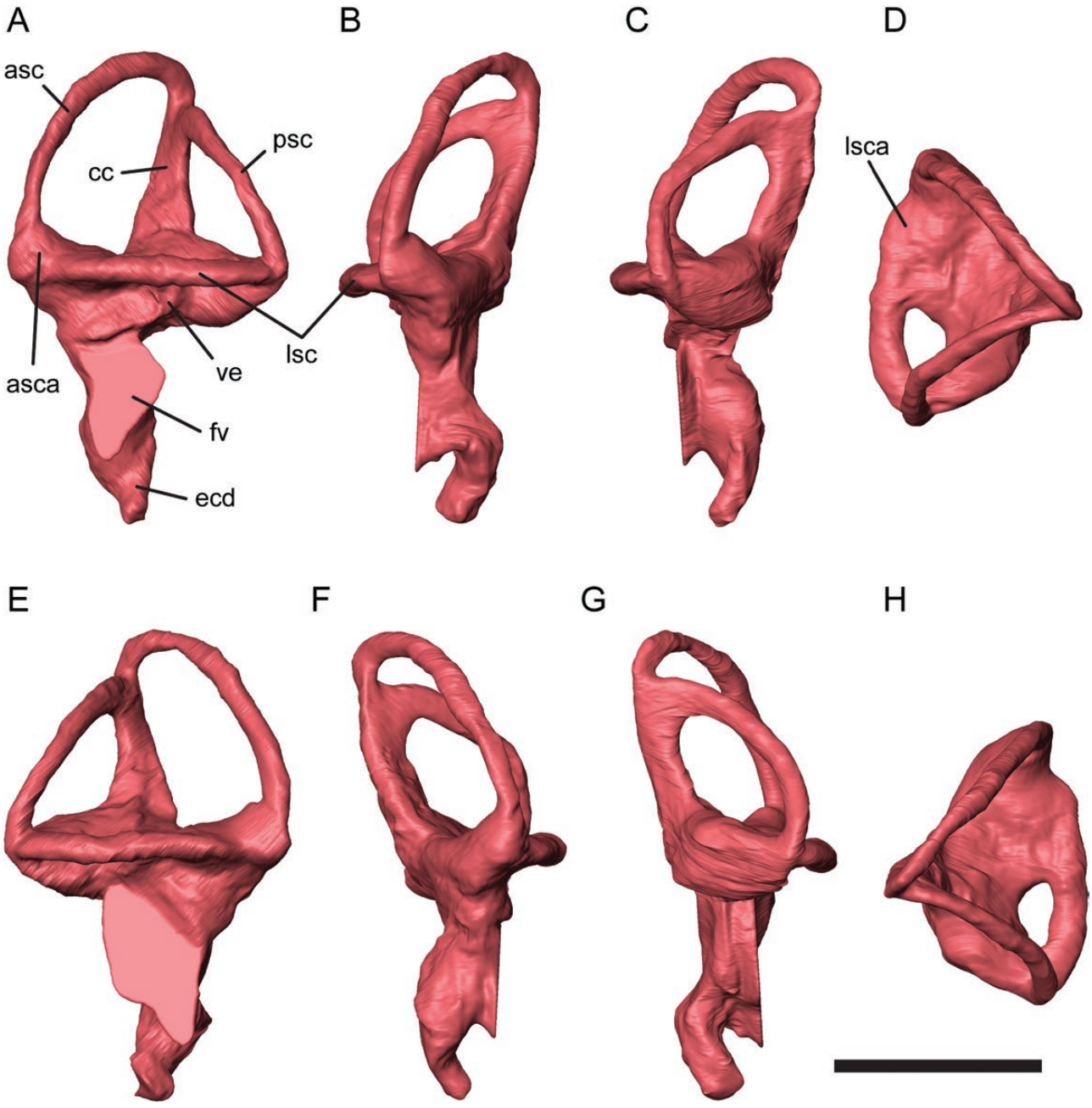

Figure 9. Model of the labyrinths of *Thecodontosaurus antiquus*, specimen YPM 2192. A–D, left labyrinth in lateral (A), anterior (B), posterior (C) and dorsal (D) views. E–H, right labyrinth in lateral (E), anterior (F), posterior (G) and dorsal (H) views. Abbreviations: asc, anterior semicircular canal; asca, ampulla of the anterior semicircular canal; cc, crus commune; ecd, endosseous cochlear duct; fv, foramen vestibuli; lsc, lateral semicircular canal; lsca, ampulla of the lateral semicircular canal; psc, posterior semicircular canal; ve, vestibule. Scale bar: 1 cm.

1990; Bronzati *et al.*, 2017), the flocculi of YPM 2192 are prominent compared with those of sauropods (Chatterjee & Zheng, 2002; Knoll & Schwarz-Wings, 2009; Balanoff *et al.*, 2010; Knoll *et al.*, 2012; Paulina Carabajal, 2012; Bronzati *et al.*, 2018a), entering the ASC. Prominent flocculi are lost in more derived Sauropodomorpha to the point that they are almost imperceptible in derived Sauropoda and become rare or cannot be detected in sauropod endocasts (Witmer *et al.*, 2008; Paulina Carabajal, 2012; Knoll *et al.*, 2012). Dorsally, the cerebellum of *Thecodontosaurus* is constricted, forming an hourglass shape with the

flocculi and medulla oblongata (Fig. 8A, E). Unlike some more derived sauropods, YPM 2192 lacks a dural expansion along the dorsal cerebellum (Witmer *et al.*, 2008; Knoll *et al.*, 2012; Sues *et al.*, 2015). The medulla oblongata forms a 128° pontine flexure angle with the rest of the cerebellum anteriorly and exits the braincase as a large, circular feature posteriorly.

Ventrally, the main body of the endocast has a smooth, rounded appearance. Cranial nerves are the only notable anatomy present along the ventral surface of the endocast. Anteriorly, the trigeminal nerve (CN V) is the largest of all and projects venterolaterally from both sides of the endocast (Fig. 8B, C). Immediately posterior to CN V is the foramen for the facial nerve (CN VII). The posteriormost cranial nerve, the hypoglossal nerve (CN XII), is represented by two diminutive foramina nearest the medulla oblongata (Fig. 8B, C). In the earlier interpretations of the endocast of YPM 2192, Benton *et al.* (2000: fig. 6G) depicted the abducens nerve (CN VI) as being located directly ventral to CN V, but CN VI could not be located in the CT data. This indicates that CN VI was not preserved well enough to be reconstructed or that CN VI was located anteroventrally to CN V and not preserved at all.

Ventral to the main body of the endocast, a partial cast of the pituitary is preserved (Fig. 8B–F). The total size of the pituitary cannot be determined, but its widest point is one-third the size of the anterior cross-section of the endocast. This indicates that the complete pituitary was large relative to the rest of the endocast; a common trait among sauropods (Knoll *et al.*, 2012). The ventralmost extent of the pituitary is marked by the laterally situated internal carotid arteries (Fig. 8F).

Endosseous labyrinth

The endosseous labyrinth of *Thecodontosaurus* (Fig. 9) is generally similar in shape to those of other sauropodomorph dinosaurs, such as *Massospondylus*, *Plateosaurus*, *Sarahsaurus* Rowe, Sues & Reisz, 2011 and *Saturnalia* (Bronzati *et al.*, 2017; Marsh & Rowe, 2018; Neenan *et al.*, 2018). However, it presents a particularly tall aspect ratio, with its total height being 1.7 times greater than its width.

The ASC is by far the longest and tallest of the three semicircular canals (Table 1), reaching far dorsally. The ASC is connected to the vestibule via the ampulla of the ASC and extends in a gentle arc dorsomedially until a sharp ventral curve, where it meets the crus commune. The PSC, in contrast, is shorter and does not extend further dorsally than the crus commune, as the ASC does. The PSC, as in other sauropodomorphs, has notable sinusoidal curvature, bowing out laterally in dorsal view, and appears to terminate where it meets the LSC. However, the soft tissue structure that sits within the PSC, the posterior semicircular duct, would have continued past this point in a medioventral curve to meet an ampulla that cannot be seen from the endosseous reconstruction, as discussed by Neenan *et al.* (2018) and Evers *et al.* (2019). The LSC is the shortest and widest of the semicircular canals and extends from a large ampulla at the anterior portion of the vestibule in a gentle curve posteromedially. However, once it reaches the PSC, it curves more sharply, passing under the PSC towards the crus commune. The crus commune is relatively wide and rotates slightly around the vertical axis so that its dorsal portion faces more anteriorly than it does at its base.

Unusually for a sauropodomorph, the endosseous cochlear duct (ECD) is well preserved in *Thecodontosaurus*. It is relatively long at 9.3 mm (Table 1) and has a large fenestra vestibuli at its dorsolateral margin. The ECD is wide but tapers to a relatively narrow tip. This tip curves distinctly laterally, in contrast to the wider main body of the ECD, which generally points posteroventrally.

Auditory function

The conservative maximal hearing range and average hearing frequency for YPM 2192 were calculated to be 3089 and 1893 Hz, respectively, based on the cochlear duct and basicranial lengths of the cranium. This indicates that any inter- or intraspecific communication for the species occurred at ~1900 Hz or, maximally, less than double that for the species. We cannot compare these values with those for other basal sauropodomorphs because they have not been calculated; therefore, we cannot say whether YPM 2192 had unusual or expected hearing ability.

DISCUSSION

Braincase anatomy

Our redescription of YPM 2192, based on tomographic data, reveals new information about the braincase anatomy of *T. antiquus* and the early evolution of braincase morphology in Sauropodomorpha. *Thecodontosaurus* shares a series of traits with other basal sauropodomorphs, such as the presence of basioccipital components of the basal tubera medial to the parabasisphenoidal components and a concave basioccipital–parabasisphenoid suture in ventral view (Bronzati & Rauhut, 2017). A lateral unossified gap on the basioccipital–parabasisphenoid–otoccipital junction seen in YPM 2192 is also present in other basal sauropodomorphs (Bronzati & Rauhut, 2017), but not in *Saturnalia* (Bronzati *et al.*, 2018b), suggesting that this trait might have evolved in the ancestor of the

clade formed by *Thecodontosaurus* and more derived sauropodomorphs.

The alignment of the cultriform process, the base of the basipterygoid processes and the occipital condyle results in a straight ventral margin of the braincase, similar to *Efraasia* (Bronzati & Rauhut, 2017) and *Adeopapposaurus* (Martínez, 2009). A 'stepped' braincase morphology is present in other taxa, such as *Saturnalia* (Bronzati *et al.*, 2018b), *Unaysaurus* (McPhee *et al.*, 2020) and *Massospondylus* (Chapelle & Choiniere, 2018), with a particularly pronounced offset of the basioccipital condyle in *Plateosaurus* (Prieto-Márquez & Norell, 2011), *Coloradisaurus* (Apaldetti *et al.*, 2014) and *Lufengosaurus* (Barrett *et al.*, 2005). The variability of this character among sauropodomorphs makes it ineffective to establish phylogenetic relationships and complicates the interpretation of the plesiomorphic condition for Sauropodomorpha.

Other features that characterize YPM 2192 are a rhomboid foramen magnum and basipterygoid processes forming a right angle with the cultriform process, the latter also seen in *Adeopapposaurus* (Martínez, 2009). The notch for the exit of vena occipitalis externa on the anterodorsal margin of the supraoccipital is remarkably shallow in YPM 2192. These notches become deeper in *Panphagia* (Martínez *et al.*, 2012) and *Massospondylus* (Chapelle & Choiniere, 2018) and are completely enclosed by the supraoccipital in *Coloradisaurus* (Apaldetti *et al.*, 2014). As discussed by Sampson & Witmer (2007), the vena cerebralis media becomes the vena occipitalis externa when it exits the braincase posteriorly, either through the supraoccipital or through the notch at the supraoccipital–parietal suture. The vena cerebralis media also has an exit on the lateral wall of the braincase and through a distinct foramen in most sauropodomorphs. The foramen for this vein is located posterodorsal to the trigeminal foramen in YPM 2192 and in *Efraasia* (Bronzati & Rauhut, 2017) and anterodorsal to it in sauropods, such as *Spinophorosaurus* Remes *et al.*, 2009 (Knoll *et al.*, 2012) and *Shunosaurus* Dong, Zhou & Zhang, 1983 (Chatterjee & Zheng, 2002). In contrast, the vena cerebralis media exits the braincase laterally, through the trigeminal foramen, in *Coloradisaurus* (Apaldetti *et al.*, 2014; Bronzati & Rauhut, 2017).

The metotic foramen is undivided in YPM 2192, a condition also seen in an isolated otoccipital from Tytherington (Ballell *et al.*, 2020). This feature is also present in *Plateosaurus* (Prieto-Márquez & Norell, 2011) and sauropods (Chatterjee & Zheng, 2002; Knoll *et al.*, 2012; Bronzati & Rauhut, 2017; Bronzati *et al.*, 2018a), whereas in some non-sauropodan taxa, such as *Coloradisaurus* (Apaldetti *et al.*, 2014), *Efraasia* (Bronzati & Rauhut, 2017) and *Melanorosaurus* (Yates, 2007), a bony strut divides the metotic foramen into two openings. An undivided metotic fissure (e.g. in sauropods) could indicate that the vena cephalica posterior exited the skull through the foramen magnum, as seen in some crocodilians and lepidosaurs (Gower, 2002; Sobral *et al.*, 2012; Bronzati & Rauhut, 2017).

Neuroanatomy and palaeobiology of *Thecodontosaurus*

Digital preparation of the YPM 2192 braincase has revealed valuable information on the neuroanatomy of *Thecodontosaurus*. A remarkable feature of the endocast is the presence of large floccular fossae that would have housed voluminous flocculi. These cerebellar lobes, via connections to the vestibular system and the eye and neck musculature, mediate two gaze- and head-stabilizing autonomic reflexes: the vestibulo-ocular reflex (VOR) and the vestibulocollic reflex (VCR) (Winship & Wylie, 2003; Witmer *et al.*, 2003; Cullen, 2012). Using sensory inputs from the vestibular and visual systems, the VOR stabilizes the eyes during head movements (Gioanni, 1988; Cullen, 2012) and the VCR maintains head position against body motions (Gioanni, 1988; Goldberg & Cullen, 2011) by activating eye and neck muscles, respectively. By adjusting and stabilizing gaze during locomotion, these reflexes play an important role in different aspects of animal behaviour, such as escape, foraging and hunting. As a fundamental integration centre within the VOR and VCR pathways, it has been suggested that flocculus size is related to locomotor performance, with large flocculi reflecting enhanced agility and motion complexity (Witmer *et al.*, 2003). This assumption is sometimes problematic, because enlargement of the floccular fossae can be caused by an increase in size of parts of the cerebellum other than the flocculus and is not correlated with aerial locomotion in extant birds (Walsh *et al.*, 2013; Ferreira-Cardoso *et al.*, 2017). However, Walsh *et al.* (2013) suggested that larger floccular fossae in flightless birds might be related to functional demands related to bipedal locomotion. In mammals, the size of the paraflocculi, which occupy the floccular fossae and control the VOR and VCR, is related to locomotory style and agility in some groups (Bertrand *et al.*, 2018, 2019, 2020; Lang *et al.*, 2018). Despite the lack of a clear correlation with behaviour and the influence of phylogeny (Ferreira-Cardoso *et al.*, 2017), a link between floccular fossa size and balance and agility can be inferred logically in specific scenarios, especially when inferences are complemented by evidence from other parts of the anatomy. In the context of sauropodomorph palaeobiology, floccular

lobe size has been associated with stance, because basal sauropodomorphs exhibit large flocculi (Bronzati *et al.*, 2017), whereas in sauropods these are greatly reduced or absent (Chatterjee & Zheng, 2002; Knoll & Schwarz-Wings, 2009; Balanoff *et al.*, 2010; Knoll *et al.*, 2012; Paulina Carabajal, 2012; Bronzati *et al.*, 2018a), suggesting that this reduction could be associated with a switch to quadrupedality. Other interpretations for large flocculi in dinosaurs include predatory and complex social behaviours (Lautenschlager *et al.*, 2012), and the former has been proposed to explain this condition in basal sauropodomorphs, such as *Saturnalia* (Bronzati *et al.*, 2017).

The labyrinth of *Thecodontosaurus* is remarkably well preserved, showing large semicircular canals, with the anterior canal being particularly prominent. The size of the ASC in relationship to skull length and head mass is a good proxy to separate putatively bipedal and quadrupedal dinosaur taxa (Georgi *et al.*, 2013). Unfortunately, *Thecodontosaurus* skull material is not sufficiently complete to enable estimation of the skull dimensions (Benton *et al.*, 2000; Ballell *et al.*, 2020), and thus quantitative comparisons cannot be made with other taxa. However, comparisons of labyrinth morphology with other sauropodomorphs (Knoll *et al.*, 2012; Neenan *et al.*, 2018) suggest that *Thecodontosaurus* had a relatively large ASC, as in other basal members of this clade.

The endocranial configuration of *Thecodontosaurus*, when interpreted together with its general osteology, provides important information about the palaeobiology of the species. The first reconstructions of *Thecodontosaurus* showed it in a crouched, quadrupedal posture (von Huene, 1932), although recent descriptions of its appendicular skeleton indicate that it was a biped (Benton *et al.*, 2000; Ballell *et al.*, 2020), the generalized stance among basal sauropodomorphs (Carrano, 2000; Carrano *et al.*, 2005; McPhee *et al.*, 2018; Chapelle *et al.*, 2020). In fact, its pelvic girdle and hindlimb show plesiomorphic features that indicate that *Thecodontosaurus* was a cursorial and agile dinosaur (Ballell *et al.*, 2020), lacking the modifications related to the more graviportal locomotion of derived sauropodomorphs (Yates *et al.*, 2010; Kubo & Kubo, 2012; Tsai & Holliday, 2015; McPhee & Choiniere, 2016; Müller *et al.*, 2018; Tsai *et al.*, 2018). Although no complete skull has been found, maxillary and dentary teeth of *Thecodontosaurus* show straight and lanceolate crowns with coarse, oblique serrations (Benton *et al.*, 2000; Ballell *et al.*, 2020). This morphology differs from that of Carnian sauropodomorphs, which have laterally compressed, posteriorly curved and finely serrated teeth and a diversity of dental features that indicate they were carnivores or omnivores (Sereno *et al.*, 2013; Bronzati *et al.*, 2017, 2019; Müller & Garcia, 2019). Although less coarsely serrated, the teeth of *Thecodontosaurus* are more similar to those of *Plateosaurus* and other basal plateosaurians (Gow *et al.*, 1990; Prieto-Márquez & Norell, 2011; McPhee *et al.*, 2020; Müller, 2020). This tooth morphology has traditionally been associated with herbivory, but it is currently accepted that these taxa engaged in facultative omnivory (Barrett, 2000; Barrett & Upchurch, 2007; Button *et al.*, 2016). In this context, the morphology of the flocculi and labyrinth is additional evidence for bipedalism in *Thecodontosaurus* and suggests that it was an active and agile sauropodomorph capable of rapid head movements along with a stable gaze while moving. Although its tooth morphology indicates a predominantly herbivorous diet (Ballell *et al.*, 2020), it would have benefited from its enhanced gaze stabilization mechanisms and cursoriality to engage occasionally in faunivory and hunt small prey.

Estimations of auditory capabilities in non-avian dinosaurs yield similar results across different lineages and show that hearing was specialized for low to middle frequencies (Gleich *et al.*, 2005; Witmer *et al.*, 2008; Evans *et al.*, 2009; Walsh *et al.*, 2009; Lautenschlager *et al.*, 2012; Paulina-Carabajal *et al.*, 2016). Our calculations indicate that the auditory abilities of *Thecodontosaurus* are congruent with these ranges, although its hearing was adapted to slightly higher frequencies than in lambeosaurines (Evans *et al.*, 2009) and sauropods (Witmer *et al.*, 2008), and its average hearing frequency was slightly higher than in therizinosaurs (Lautenschlager *et al.*, 2012) and close to *Archaeopteryx* Meyer, 1861 (Gleich *et al.*, 2005; Walsh *et al.*, 2009). Both hearing ranges were less than those calculated for the predatory maniraptoran, *Velociraptor* Osborn, 1924 (King *et al.*, 2020). Although not remarkably different from other non-avian dinosaurs, the slightly higher auditory sensitivity and complexity of *Thecodontosaurus* might reveal peculiarities of its palaeobiology. In extant saurians, ECD length is correlated with social behaviour and vocal complexity (Walsh *et al.*, 2009); therefore, the hearing frequency of *Thecodontosaurus* might suggest some degree of social aggregation. The taphonomy of the fissure fill localities where *Thecodontosaurus* was found is in accordance with this interpretation, because remains of numerous individuals of different sizes are found in close association (Benton *et al.*, 2000; Whiteside & Marshall, 2008; Ballell *et al.*, 2020), although it cannot be said whether these assemblages represent evidence for herd living or are taphonomic. Small social aggregations might have been beneficial in the peculiar palaeoenvironmental setting of the fissure localities of south-western Britain, reconstructed as a shallow sea archipelago of small and endemic islands, housing a rich vertebrate fauna (Whiteside & Marshall, 2008; Whiteside *et al.*, 2016).

Endocranial evolution in Sauropodomorphs

Sauropodomorphs underwent drastic changes in their biology and ecology throughout their evolution (Barrett, 2000, 2014; Carrano, 2005; Barrett & Upchurch, 2007; Sander *et al.*, 2011; Sander, 2013; Button *et al.*, 2014, 2016, 2017; Cabreira *et al.*, 2016; McPhee *et al.*, 2018). Modifications of their cranial and postcranial anatomy permitted shifts in diet (Barrett, 2000; Barrett & Upchurch, 2007; Button *et al.*, 2016; Cabreira *et al.*, 2016; Müller *et al.*, 2018; Bronzati *et al.*, 2019; Müller & Garcia, 2019), locomotion (Carrano, 2005; McPhee *et al.*, 2018; Otero *et al.*, 2019; Chapelle *et al.*, 2020) and behaviour that triggered the acquisition of gigantic body sizes in sauropods (Sander *et al.*, 2011; Sander, 2013). Previous research has indicated that many of these shifts were also apparent in the shape of the endocranial cavity, where the endocranial soft tissue would have been during life (Knoll *et al.*, 2012; Paulina Carabajal, 2012; Bronzati *et al.*, 2017; Neenan *et al.*, 2018). Although the endocast of YPM 2192 is restricted to the hindbrain, there are key features that are of interest to the endocranial macroevolution of sauropodomorphs: the flocculi, endosseous labyrinths and pontine flexure.

Although the pontine flexure of YPM 2192 cannot be measured properly owing to the missing telencephalon, the hindbrain (and therefore the rest of the endocast) does not lie along the same plane. This is similar to the hindbrains of *Saturnalia tupiniquim* Langer, Abdala, Richter & Benton, 1999 and *Plateosaurus engelhardti* von Meyer, 1837 (Bronzati *et al.*, 2017) in that the hindbrain makes an abrupt flexure change immediately posterior to the flocculi. Given that the pontine flexure is < ~180° in basal sauropodomorphs (and even in derived sauropods), this is a big change from the flattened, elongated brain of phytosaurs and non-dinosaurian archosaurs (Lautenschlager & Butler, 2016; Nesbitt *et al.*, 2017), orientated all along the same plane, and the change occurred early on in the evolution of Sauropodomorpha.

The flocculi of YPM 2192 are of special interest among basal sauropodomorphs because of their transitional appearance, because flocculi are associated with agility, locomotion, the VOR and VCR (Hopson, 1977; Witmer *et al.*, 2003; Witmer & Ridgely, 2009). Although great care should be taken when assuming how much the flocculi govern the previously mentioned cranial and somatic controls (Walsh *et al.*, 2013; Ferreira-Cardoso *et al.*, 2017), the reduction in floccular size between basal sauropodomorphs and derived sauropods is clear. Bronzati *et al.* (2017) pointed out that the reduction in floccular size began well before the origin of sauropods. The floccular lobes of *T. antiquus* are

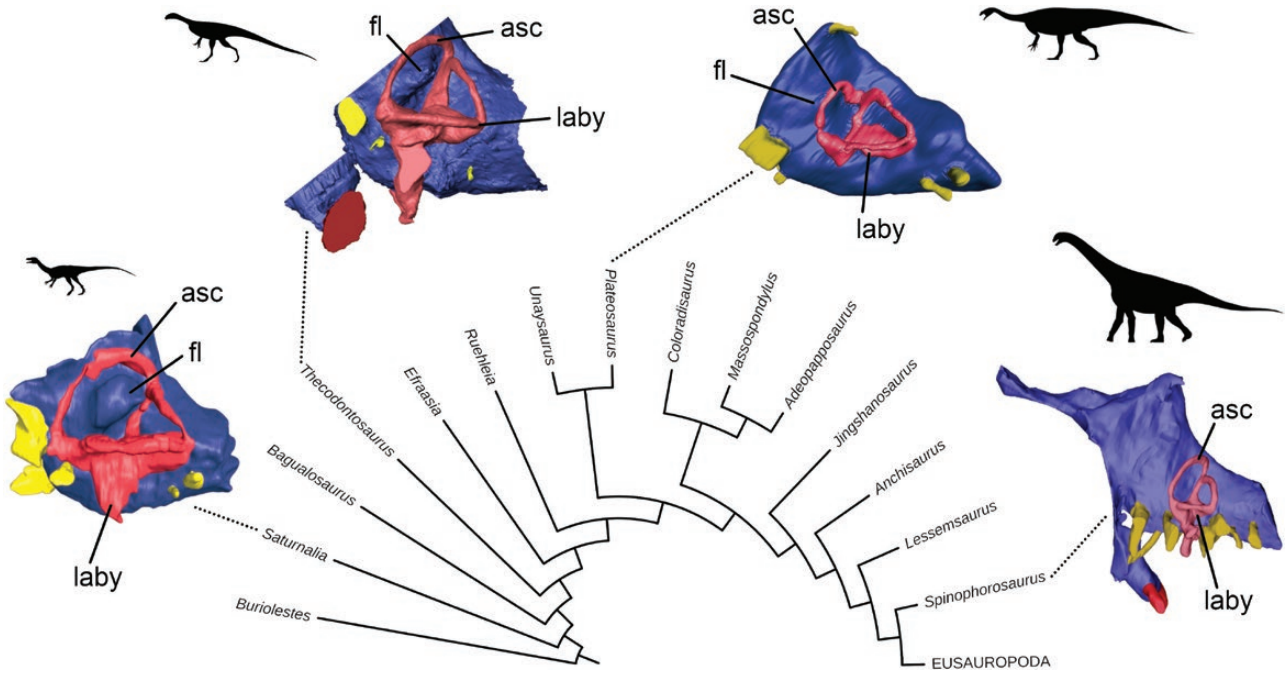

Figure 10. Evolution of endocranial morphology in Sauropodomorpha. Endocasts are in lateral view and not to scale. Abbreviations: asc, anterior semicircular canal; fl, floccular lobe; laby, endosseous labyrinth. The simplified phylogeny of Sauropodomorpha is based on the studies by Remes *et al.* (2009), Otero & Pol (2013), Langer *et al.* (2019) and McPhee *et al.* (2020). *Saturnalia* and *Plateosaurus* endocasts are from the study by Bronzati *et al.* (2017); *Spinophorosaurus* endocast is from the study by Knoll *et al.* (2012). The phylogenetic tree was edited in iTOL v.5 (https://itol.embl.de). Silhouettes are from http://phylopic.org

reduced in comparison to those of *S. tupiniquim*, in that the flocculi of YPM 2192 do not reach the crus commune of the labyrinths (Fig. 10). Furthermore, the flocculi of *P. engelhardti* are even more reduced when compared with those in *T. antiquus*. YPM 2192 shows when the flocculi began their reduction within Sauropodomorpha (Fig. 10), ~30 Myr after the first unequivocal record of a sauropodomorph. However, note that *Thecodontosaurus* is an anachronistic holdover in its island home, showing affinities with late Carnian and early Norian sauropodomorphs, although it is Rhaetian in age (Whiteside *et al.*, 2016).

The ASC of YPM 2192 is similar to those of other basal non-sauropodan sauropodomorphs and basal titanosauriforms in that it is enlarged when compared with the PSC (Knoll *et al.*, 2012). This means that, in terms of balance and agility, the flocculi became reduced long before the ASC became more rounded and oblate when compared with the PSC, as observed in more derived eusauropods (Knoll *et al.*, 2012). Unfortunately, we cannot say when the endocast and peripheral endosseous anatomy became reduced, because of the scarcity of associated braincases and limb elements from basal sauropods. Furthermore, this means we cannot determine whether the brain and inner ear changed at the same time or not.

To summarize, the endocast and endosseous labyrinths of YPM 2192 are most like those of basal non-sauropodan sauropodomorphs in that the flocculi are large when compared with sauropods, the ASC is elongate and is longer than the PSC, and the brain and cranial nerves do not all lie along the same plane. However, the *Thecodontosaurus* endocast shows that the transition to the sauropodan configuration, where the flocculi shrank and no longer contacted the internal wall of the braincase, began early in sauropodomorph evolution. Furthermore, it is clear that the brain and cranial nerves were changing before morphological changes in the canals of the inner ear.

Conclusions

Thecodontosaurus is an iconic taxon for being the first Triassic dinosaur ever named and occupying a basal position in the phylogeny of Sauropodomorpha. Our study presents a detailed redescription of the braincase and endocranial anatomy of YPM 2192 based on CT data. *Thecodontosaurus* shares with other basal sauropodomorphs the presence of medial components of the basal tubera formed by the basioccipital and a U-shaped basioccipital–parabasisphenoid suture. Its braincase is also characterized by the straight outline of the braincase floor, an undivided metotic foramen, the presence of an unossified gap, large floccular fossae, basipterygoid processes forming a right angle with the cultriform process in lateral view and a rhomboid foramen magnum.

The well-developed flocculi and ASC of *Thecodontosaurus* are traits associated with enhanced agility and gaze and head stability, supporting other evidence that it was bipedal and cursorial. Its agility and stable gaze might also have facilitated occasional faunivory. Estimations of the auditory abilities of *Thecodontosaurus*, based on ECD length, give similar values to other non-avian dinosaurs. Its average hearing frequency is slightly higher than that of most of the taxa for which data are available, suggesting some degree of social complexity in this species. The morphology of the *Thecodontosaurus* endocast provides new information about the pattern of endocranial evolution in Sauropodomorpha, suggesting that a decrease in floccular lobe size occurred before the reduction of the ASC.

ACKNOWLEDGEMENTS

We thank Remmert Schouten and Nicole Davies for enabling the CT scanning of the braincase. We also thank Jessica A. Maisano and Tim Rowe of the University of Texas at Austin for scanning the specimen and providing the scan parameters. We thank Daniel Brinkman of the Yale Peabody Museum of Natural History for access to the specimen. We are grateful to Mario Bronzati for providing additional images of *Saturnalia* and *Plateosaurus* endocasts. The CT scanning was funded in 2005 by a Royal Society grant (2005/R1). We thank three anonymous reviewers for their comments on earlier versions of the manuscript. A.B. is funded by a NERC GW4+ Doctoral Training Partnership studentship from the Natural Environment Research Council (NE/L002434/1). J.M.N. is funded by a Leverhulme Trust Early Career Fellowship (ECF-2017-360).

REFERENCES

Apaldetti C, **Martínez RN**, **Pol D**, **Souter T. 2014.** Redescription of the skull of *Coloradisaurus brevis* (Dinosauria, Sauropodomorpha) from the Late Triassic Los Colorados Formation of the Ischigualasto-Villa Union Basin, Northwestern Argentina. *Journal of Vertebrate Paleontology* **34:** 1113–1132.

Balanoff AM, **Bever GS**, **Ikejiri T. 2010.** The braincase of *Apatosaurus* (Dinosauria: Sauropoda) based on computed tomography of a new specimen with comments on variation and evolution in sauropod neuroanatomy. *American Museum Novitates* **3677:** 1–29.

Ballell A, **Rayfield EJ**, **Benton MJ. 2020.** Osteological redescription of the Late Triassic sauropodomorph dinosaur

Thecodontosaurus antiquus based on new material from Tytherington, southwestern England. *Journal of Vertebrate Paleontology* **40:** e1770774.

Barrett PM. 2000. Prosauropods and iguanas: speculation on the diets of extinct reptiles. In: Sues H-D, ed. *The evolution of herbivory in terrestrial vertebrates: perspectives from the fossil record*. Cambridge: Cambridge University Press, 42–78.

Barrett PM. 2014. Paleobiology of herbivorous dinosaurs. *Annual Review of Earth and Planetary Sciences* **42:** 207–230.

Barrett PM, **Butler RJ**, **Nesbitt SJ. 2011.** The roles of herbivory and omnivory in early dinosaur evolution. *Earth and Environmental Science Transactions of the Royal Society of Edinburgh* **101:** 383–396.

Barrett PM, **Rayfield EJ. 2006.** Ecological and evolutionary implications of dinosaur feeding behaviour. *Trends in Ecology & Evolution* **21:** 217–244.

Barrett PM, **Upchurch P. 2007.** The evolution of feeding mechanisms in early sauropodomorph dinosaurs. *Special Papers in Palaeontology* **77:** 91–112.

Barrett PM, **Upchurch P**, **Xiao-Lin W. 2005.** Cranial osteology of *Lufengosaurus huenei* Young (Dinosauria: Prosauropoda) from the Lower Jurassic of Yunnan, People's Republic of China. *Journal of Vertebrate Paleontology* **25:** 806–822.

Benton MJ. 2012. Naming the Bristol dinosaur, *Thecodontosaurus*: politics and science in the 1830s. *Proceedings of the Geologists' Association* **123:** 766–778.

Benton MJ, **Juul L**, **Storrs GW**, **Galton PM. 2000.** Anatomy and systematics of the prosauropod dinosaur *Thecodontosaurus antiquus* from the Upper Triassic of southwest England. *Journal of Vertebrate Paleontology* **20:** 77–108.

Bertrand OC, **Amador-Mughal F**, **Lang MM**, **Silcox MT. 2018.** Virtual endocasts of fossil Sciuroidea: brain size reduction in the evolution of fossoriality. *Palaeontology* **61:** 919–948.

Bertrand OC, **San Martin-Flores G**, **Silcox MT. 2019.** Endocranial shape variation in the squirrel-related clade and their fossil relatives using 3D geometric morphometrics: contributions of locomotion and phylogeny to brain shape. *Journal of Zoology* **308:** 197–211.

Bertrand OC, **Shelley SL**, **Wible JR**, **Williamson TE**, **Holbrook LT**, **Chester SGB**, **Butler IB**, **Brusatte SL. 2020.** Virtual endocranial and inner ear endocasts of the Paleocene 'condylarth' *Chriacus*: new insight into the neurosensory system and evolution of early placental mammals. *Journal of Anatomy* **236:** 21–49.

Bittencourt JS, **Arcucci AB**, **Marsicano CA**, **Langer MC. 2015.** Osteology of the Middle Triassic archosaur *Lewisuchus admixtus* Romer (Chañares Formation, Argentina), its inclusivity, and relationships amongst early dinosauromorphs. *Journal of Systematic Palaeontology* **13:** 189–219.

Bronzati M, **Benson RBJ**, **Rauhut OWM. 2018a.** Rapid transformation in the braincase of sauropod dinosaurs: integrated evolution of the braincase and neck in early sauropods? *Palaeontology* **61:** 289–302.

Bronzati M, **Langer MC**, **Rauhut OWM. 2018b.** Braincase anatomy of the early sauropodomorph *Saturnalia tupiniquim* (Late Triassic, Brazil). *Journal of Vertebrate Paleontology* **38:** e1559173.

Bronzati M, **Müller RT**, **Langer MC. 2019.** Skull remains of the dinosaur *Saturnalia tupiniquim* (Late Triassic, Brazil): with comments on the early evolution of sauropodomorph feeding behavior. *PLoS One* **14:** e0221387.

Bronzati M, **Rauhut OWM. 2017.** Braincase redescription of *Efraasia minor* Huene, 1908 (Dinosauria: Sauropodomorpha) from the Late Triassic of Germany, with comments on the evolution of the sauropodomorph braincase. *Zoological Journal of the Linnean Society* **182:** 173–224.

Bronzati M, **Rauhut OWM**, **Bittencourt JS**, **Langer MC. 2017.** Endocast of the Late Triassic (Carnian) dinosaur *Saturnalia tupinquim*: implications for the evolution of brain tissue in Sauropodomorpha. *Scientific Reports* **7:** 11931.

Button DJ, **Barrett PM**, **Rayfield EJ. 2016.** Comparative cranial myology and biomechanics of *Plateosaurus* and *Camarasaurus* and evolution of the sauropod feeding apparatus. *Palaeontology* **59:** 887–913.

Button DJ, **Barrett PM**, **Rayfield EJ. 2017.** Craniodental functional evolution in sauropodomorph dinosaurs. *Paleobiology* **43:** 435–462.

Button DJ, **Rayfield EJ**, **Barrett PM. 2014.** Cranial biomechanics underpins high sauropod diversity in resource-poor environments. *Proceedings of the Royal Society B: Biological Sciences* **281:** 20142114.

Cabreira SF, **Kellner AWA**, **Dias-da-Silva S**, **da Silva LR**, **Bronzati M**, **Marsola JCA**, **Müller RT**, **Bittencourt JS**, **Batista BJ**, **Raugust T**, **Carrilho R**, **Brodt A**, **Langer MC. 2016.** A unique Late Triassic dinosauromorph assemblage reveals dinosaur ancestral anatomy and diet. *Current Biology* **26:** 3090–3095.

Carrano MT. 1999. What, if anything, is a cursor? Categories versus continua for determining locomotor habit in mammals and dinosaurs. *Journal of Zoology* **247:** 29–42.

Carrano MT. 2000. Homoplasy and the evolution of dinosaur locomotion. *Paleobiology* **26:** 489–512.

Carrano MT. 2005. The evolution of sauropod locomotion. In: Curry Rogers KA, Wilson JA, eds. *The sauropods: evolution and paleobiology*. Berkeley: University of California Press, 229–250.

Chapelle KEJ, **Benson RBJ**, **Stiegler J**, **Otero A**, **Zhao Q**, **Choiniere JN. 2020.** A quantitative method for inferring locomotory shifts in amniotes during ontogeny, its application to dinosaurs and its bearing on the evolution of posture. *Palaeontology* **63:** 229–242.

Chapelle KEJ, **Choiniere JN. 2018.** A revised cranial description of *Massospondylus carinatus* Owen (Dinosauria: Sauropodomorpha) based on computed tomographic scans and a review of cranial characters for basal Sauropodomorpha. *PeerJ* **6:** e4224.

Chatterjee S, **Zheng Z. 2002.** Cranial anatomy of *Shunosaurus*, a basal sauropod dinosaur from the Middle Jurassic of China. *Zoological Journal of the Linnean Society* **136:** 145–169.

Cullen KE. 2012. The vestibular system: multimodal integration and encoding of self-motion for motor control. *Trends in Neurosciences* **35:** 185–196.

Dutel H, **Galland M**, **Tafforeau P**, **Long JA**, **Fagan MJ**, **Janvier P**, **Herrel A**, **Santin MD**, **Clément G**, **Herbin M. 2019.** Neurocranial development of the coelacanth and the evolution of the sarcopterygian head. *Nature* **569:** 556–559.

Evans DC, **Ridgely R**, **Witmer LM. 2009.** Endocranial anatomy of lambeosaurine hadrosaurids (Dinosauria: Ornithischia): a sensorineural perspective on cranial crest function. *Anatomical Record* **292:** 1315–1337.

Evers SW, **Neenan JM**, **Ferreira GS**, **Werneburg I**, **Barrett PM**, **Benson RBJ. 2019.** Neurovascular anatomy of the protostegid turtle *Rhinochelys pulchriceps* and comparisons of membranous and endosseous labyrinth shape in an extant turtle. *Zoological Journal of the Linnean Society* **187:** 800–828.

Ferreira-Cardoso S, **Araujo R**, **Martins NE**, **Martins GG**, **Walsh S**, **Martins RMS**, **Kardjilov N**, **Manke I**, **Hilger A**, **Castanhinha R. 2017.** Floccular fossa size is not a reliable proxy of ecology and behaviour in vertebrates. *Scientific Reports* **7:** 2005.

Galton PM. 1985. Cranial anatomy of the prosauropod dinosaur *Plateosaurus* from the Knollenmergel (Middle Keuper, Upper Triassic) of Germany. *Geologica et Palaeontologica* **19:** 119–159.

Galton PM, **Kermack D. 2010.** The anatomy of *Pantydraco caducus*, a very basal sauropodomorph dinosaur from the Rhaetian (Upper Triassic) of South Wales, UK. *Revue de Paléobiologie* **29:** 341–404.

Gauthier J. 1986. Saurischian monophyly and the origin of birds. *Memoirs of the California Academy of Sciences* **8:** 1–55.

Georgi JA, **Sipla JS**, **Forster CA. 2013.** Turning semicircular canal function on its head: dinosaurs and a novel vestibular analysis. *PLoS One* **8:** e58517.

Gioanni H. 1988. Stabilizing gaze reflexes in the pigeon (*Columba livia*). II. Vestibulo-ocular (VOR) and vestibulo-collic (closed-loop VCR) reflexes. *Experimental Brain Research* **69:** 583–593.

Gleich O, **Dooling RJ**, **Manley GA. 2005.** Audiogram, body mass, and basilar papilla length: correlations in birds and predictions for extinct archosaurs. *Naturwissenschaften* **92:** 595–598.

Goldberg JM, **Cullen KE. 2011.** Vestibular control of the head: possible functions of the vestibulocollic reflex. *Experimental Brain Research* **210:** 331–345.

Gow CE. 1990. Morphology and growth of the *Massospondylus* braincase (Dinosauria, Prosauropoda). *Palaeontologia Africana* **27:** 59–75.

Gow CE, **Kitching JW**, **Raath MA. 1990.** Skulls of the prosauropod dinosaur *Massospondylus carinatus* Owen in the collections of the Bernard Price Institute for Palaeontological Research. *Palaeontologia Africana* **27:** 45–58.

Gower DJ. 2002. Braincase evolution in suchian archosaurs (Reptilia: Diapsida): evidence from the rauisuchian *Batrachotomus kupferzellensis*. *Zoological Journal of the Linnean Society* **136:** 49–76.

Holliday CM, **Witmer LM. 2009.** The epipterygoid of crocodyliforms and its significance for the evolution of the orbitotemporal region of eusuchians. *Journal of Vertebrate Paleontology* **29:** 715–733.

Hopson J. 1977. Relative brain size and behavior in archosaurian reptiles. *Annual Review of Ecology and Systematics* **8:** 429–448.

von Huene F. 1932. Die fossile Reptil-Ordnung Saurischia, ihre Entwicklung und Geschichte. *Monographien zur Geologie und Paläontologie* **4:** 1–361.

Jirak D, **Janacek J. 2017.** Volume of the crocodilian brain and endocast during ontogeny. *PLoS One* **12:** e0178491.

King JL, **Sipla JS**, **Georgi JA**, **Balanoff AM**, **Neenan JM. 2020.** The endocranium and trophic ecology of *Velociraptor mongoliensis*. *Journal of Anatomy* **237:** 861–869.

Knoll F, **Schwarz-Wings D. 2009.** Palaeoneuroanatomy of *Brachiosaurus*. *Annales de Paléontologie* **95:** 165–175.

Knoll F, **Witmer LM**, **Ortega F**, **Ridgely RC. 2012.** The braincase of the basal sauropod dinosaur *Spinophorosaurus* and 3D reconstructions of the cranial endocast and inner ear. *PLoS One* **7:** e30060.

Kubo T, **Kubo MO. 2012.** Associated evolution of bipedality and cursoriality among Triassic archosaurs: a phylogenetically controlled evaluation. *Paleobiology* **38:** 474–485.

Lang MM, **Bertrand OC**, **Silcox MT. 2018.** Scaling patterns of primate paraflocculi: effects of phylogeny and ecology. *American Journal of Physical Anthropology* **165:** 152.

Langer MC, **McPhee BW**, **Marsola JCD**, **Roberto-da-Silva L**, **Cabreira SF. 2019.** Anatomy of the dinosaur *Pampadromaeus barberenai* (Saurischia—Sauropodomorpha) from the Late Triassic Santa Maria Formation of southern Brazil. *PLoS One* **14:** e0212543.

Lautenschlager S, **Butler RJ. 2016.** Neural and endocranial anatomy of Triassic phytosaurian reptiles and convergence with fossil and modern crocodylians. *PeerJ* **4:** e2251.

Lautenschlager S, **Rayfield EJ**, **Altangerel P**, **Zanno LE**, **Witmer LM. 2012.** The endocranial anatomy of Therizinosauria and its implications for sensory and cognitive function. *PLoS One* **7:** e52289.

Marsh AD, **Rowe TB. 2018.** Anatomy and systematics of the sauropodomorph *Sarahsaurus aurifontanalis* from the Early Jurassic Kayenta Formation. *PLoS One* **13:** e0204007.

Marsh OC. 1892. Notes on Triassic Dinosauria. *American Journal of Science* **43:** 543–546.

Martínez RN. 2009. *Adeopapposaurus mognai*, gen. et sp. nov. (Dinosauria: Sauropodomorpha), with comments on adaptations of basal Sauropodomorpha. *Journal of Vertebrate Paleontology* **29:** 142–164.

Martínez RN, **Haro JA**, **Apaldetti C. 2012.** Braincase of *Panphagia protos* (Dinosauria, Sauropodomorpha). *Journal of Vertebrate Paleontology* **32**(suppl. 1): 70–82.

McPhee BW, **Benson RB**, **Botha-Brink J**, **Bordy EM**, **Choiniere JN. 2018.** A giant dinosaur from the earliest Jurassic of South Africa and the transition to quadrupedality in early sauropodomorphs. *Current Biology* **28:** 3143–3151.

McPhee BW, **Bittencourt JS**, **Langer MC**, **Apaldetti C**, **Da Rosa ÁAS. 2020.** Reassessment of *Unaysaurus tolentinoi*

(Dinosauria: Sauropodomorpha) from the Late Triassic (early Norian) of Brazil, with a consideration of the evidence for monophyly within non-sauropodan sauropodomorphs. *Journal of Systematic Palaeontology* **18:** 259–293.

McPhee BW, **Choiniere JN. 2016.** A hyper-robust sauropodomorph dinosaur ilium from the Upper Triassic–Lower Jurassic Elliot Formation of South Africa: implications for the functional diversity of basal Sauropodomorpha. *Journal of African Earth Sciences* **123:** 177–184.

Miyashita T, **Arbour VM**, **Witmer LM**, **Currie PJ. 2011.** The internal cranial morphology of an armoured dinosaur *Euoplocephalus* corroborated by X-ray computed tomographic reconstruction. *Journal of Anatomy* **219:** 661–675.

Müller RT. 2020. Craniomandibular osteology of *Macrocollum itaquii* (Dinosauria: Sauropodomorpha) from the Late Triassic of southern Brazil. *Journal of Systematic Palaeontology* **18:** 805–841.

Müller RT, **Garcia MS. 2019.** Rise of an empire: analysing the high diversity of the earliest sauropodomorph dinosaurs through distinct hypotheses. *Historical Biology*. https://doi.org/10.1080/08912963.2019.1587754

Müller RT, **Langer MC**, **Dias-da-Silva S. 2018.** An exceptionally preserved association of complete dinosaur skeletons reveals the oldest long-necked sauropodomorphs. *Biology Letters* **14:** 20180633.

Neenan JM, **Chapelle KEJ**, **Fernandez V**, **Choiniere JN. 2018.** Ontogeny of the *Massospondylus* labyrinth: implications for locomotory shifts in a basal sauropodomorph dinosaur. *Palaeontology* **62:** 255–265.

Nesbitt SJ, **Sidor CA**, **Irmis RB**, **Angielczyk KD**, **Smith RMH**, **Tsuji LA. 2010.** Ecologically distinct dinosaurian sister group shows early diversification of Ornithodira. *Nature* **464:** 95–98.

Nesbitt SJ, **Stocker MR**, **Parker WG**, **Wood TA**, **Sidor CA**, **Angielczyk KD. 2017.** The braincase and endocast of *Parringtonia gracilis*, a Middle Triassic suchian (Archosaur: Pseudosuchia). *Journal of Vertebrate Paleontology* **37:** 122–141.

Otero A, **Cuff AR**, **Allen V**, **Sumner-Rooney L**, **Pol D**, **Hutchinson JR. 2019.** Ontogenetic changes in the body plan of the sauropodomorph dinosaur *Mussaurus patagonicus* reveal shifts of locomotor stance during growth. *Scientific Reports* **9:** 7614.

Otero A, **Pol D. 2013.** Postcranial anatomy and phylogenetic relationships of *Mussaurus patagonicus* (Dinosauria, Sauropodomorpha). *Journal of Vertebrate Paleontology* **33:** 1138–1168.

Paulina Carabajal A. 2012. Neuroanatomy of titanosaurid dinosaurs from the Upper Cretaceous of Patagonia, with comments on endocranial variability within Sauropoda. *Anatomical Record* **295:** 2141–2156.

Paulina-Carabajal A, **Lee YN**, **Jacobs LL. 2016.** Endocranial morphology of the primitive nodosaurid dinosaur *Pawpawsaurus campbelli* from the Early Cretaceous of North America. *PLoS One* **11:** e0150845.

Paulina-Carabajal A, **Lee YN**, **Kobayashi Y**, **Lee HJ**, **Currie PJ. 2018.** Neuroanatomy of the ankylosaurid dinosaurs *Tarchia teresae* and *Talarurus plicatospineus* from the Upper Cretaceous of Mongolia, with comments on endocranial variability among ankylosaurs. *Palaeogeography, Palaeoclimatology, Palaeoecology* **494:** 135–146.

Porro LB, **Witmer LM**, **Barrett PM. 2015.** Digital preparation and osteology of the skull of *Lesothosaurus diagnosticus* (Ornithischia: Dinosauria). *PeerJ* **3:** e1494.

Prieto-Márquez A, **Norell MA. 2011.** Redescription of a nearly complete skull of *Plateosaurus* (Dinosauria: Sauropodomorpha) from the Late Triassic of Trossingen (Germany). *American Museum Novitates* **3727:** 1–58.

Rauhut OWM. 2004. Braincase structure of the Middle Jurassic theropod dinosaur *Piatnitzkysaurus*. *Canadian Journal of Earth Sciences* **41:** 1109–1122.

Remes K, **Ortega F**, **Fierro I**, **Joger U**, **Kosma R**, **Marín Ferrer JM**, **Ide OA**, **Maga A. 2009.** A new basal sauropod dinosaur from the Middle Jurassic of Niger and the early evolution of Sauropoda. *PLoS One* **4:** e6924.

Riley H, **Stutchbury S. 1836.** A description of various fossil remains of three distinct saurian animals discovered in the autumn of 1834, in the Magnesian Conglomerate on Durdham Down, near Bristol. *Proceedings of the Geological Society of London* **2:** 397–399.

Riley H, **Stutchbury S. 1840.** A description of various fossil remains of three distinct saurian animals, recently discovered in the Magnesian Conglomerate near Bristol. *Transactions of the Geological Society of London* **5:** 349–357.

Sampson SD, **Witmer LM. 2007.** Craniofacial anatomy of *Majungasaurus crenatissimus* (Theropoda: Abelisauridae) from the Late Cretaceous of Madagascar. *Journal of Vertebrate Paleontology* **27**(suppl. 2)**:** 32–104.

Sander PM. 2013. An evolutionary cascade model for sauropod dinosaur gigantism - overview, update and tests. *PLoS One* **8:** e78573.

Sander PM, **Christian A**, **Clauss M**, **Fechner R**, **Gee CT**, **Griebeler EM**, **Gunga HC**, **Hummel J**, **Mallison H**, **Perry SF**, **Preuschoft H**, **Rauhut OWM**, **Remes K**, **Tutken T**, **Wings O**, **Witzel U. 2011.** Biology of the sauropod dinosaurs: the evolution of gigantism. *Biological Reviews* **86:** 117–155.

Sereno PC. 1997. The origin and evolution of dinosaurs. *Annual Review of Earth and Planetary Sciences* **25:** 435–489.

Sereno PC, **Martínez RN**, **Alcober OA. 2013.** Osteology of *Eoraptor lunensis* (Dinosauria, Sauropodomorpha). *Journal of Vertebrate Paleontology* **32:** 83–179.

Sereno PC, **Wilson WA**, **Witmer LM**, **Whitlock JA**, **Maga A**, **Ide O**, **Rowe TA. 2007.** Structural extremes in a Cretaceous dinosaur. *PLoS One* **2:** e1230.

Sobral G, **Hipsley CA**, **Müller J. 2012.** Braincase redescription of *Dysalotosaurus lettowvorbecki* (Dinosauria, Ornithopoda) based on computed tomography. *Journal of Vertebrate Paleontology* **32:** 1090–1102.

Sues H, **Averianov A**, **Ridgely RC**, **Witmer LM. 2015.** Titanosauria (Dinosauria, Sauropoda) from the Upper Cretaceous (Turonian) Bissekty Formation of Uzbekistan. *Journal of Vertebrate Paleontology* **35:** e889145.

Tsai HP, **Holliday CM. 2015.** Articular soft tissue anatomy of the archosaur hip joint: structural homology and functional implications. *Journal of Morphology* **276:** 601–630.

Tsai HP, **Middleton KM**, **Hutchinson JR**, **Holliday CM. 2018.** Hip joint articular soft tissues on non-dinosaurian

Dinosauromorpha and early Dinosauria: evolutionary and biomechanical implications for Saurischia. *Journal of Vertebrate Paleontology* **38:** e1427593.

Upchurch P, **Barrett PM**, **Galton PM. 2007.** A phylogenetic analysis of basal sauropodomorph relationships: implications for the origin of sauropod dinosaurs. *Special Papers in Palaeontology* **77:** 57–90.

Walsh SA, **Barrett PM**, **Milner AC**, **Manley G**, **Witmer LM. 2009.** Inner ear anatomy is a proxy for deducing auditory capability and behaviour in reptiles and birds. *Proceedings of the Royal Society B: Biological Sciences* **276:** 1355–1360.

Walsh SA, **Iwaniuk AN**, **Knoll MA**, **Bourdon E**, **Barrett PM**, **Milner AC**, **Nudds RL**, **Abel RL**, **Dello Sterpaio P. 2013.** Avian cerebellar floccular fossa size is not a proxy for flying ability in birds. *PLoS One* **8:** e67176.

Whiteside DI, **Duffin CJ**, **Gill PG**, **Marshall JEA**, **Benton MJ. 2016.** The Late Triassic and Early Jurassic fissure faunas from Bristol and South Wales: stratigraphy and setting. *Palaeontologia Polonica* **67:** 257–287.

Whiteside DI, **Marshall JEA. 2008.** The age, fauna and palaeoenvironment of the Late Triassic fissure deposits of Tytherington, South Gloucestershire, UK. *Geological Magazine* **145:** 105–147.

Winship IR, **Wylie DRW. 2003.** Zonal organization of the vestibulocerebellum in pigeons (*Columba livia*): I. Climbing fiber input to the flocculus. *Journal of Comparative Neurology* **456:** 127–139.

Witmer LM. 1997. Craniofacial air sinus systems. In: Currie PJ, Padian K, eds. *Encyclopedia of dinosaurs*. San Diego: Academic Press, 151–159.

Witmer LM, **Chatterjee S**, **Franzosa J**, **Rowe T. 2003.** Neuroanatomy of flying reptiles and implications for flight, posture and behaviour. *Nature* **425:** 950–953.

Witmer LM, **Ridgely RC. 2009.** New insights into the brain, braincase, and ear region of tyrannosaurs (Dinosauria, Theropoda), with implications for sensory organization and behavior. *Anatomical Record* **292:** 1266–1296.

Witmer LM, **Ridgely RC**, **Dufeau DL**, **Semones MC. 2008.** Using CT to peer into the past: 3D visualization of the brain and ear regions of birds, crocodiles, and nonavian dinosaurs. In: Endo H, Frey R, eds. *Anatomical imaging. Towards a new morphology*. Tokyo: Springer, 67–87.

Yates AM. 2007. The first complete skull of the Triassic dinosaur *Melanorosaurus* Haughton (Sauropodomorpha: Anchisauria). *Special Papers in Paleontology* **77:** 9–55.

Yates AM, **Bonnan MF**, **Neveling J**, **Chinsamy A**, **Blackbeard MG. 2010.** A new transitional sauropodomorph dinosaur from the Early Jurassic of South Africa and the evolution of sauropod feeding and quadrupedalism. *Proceedings of the Royal Society B: Biological Sciences* **277:** 787–794.

Yates AM, **Kitching J. 2003.** The earliest known sauropod dinosaur and the first steps towards sauropod locomotion. *Proceedings of the Royal Society B: Biological Sciences* **270:** 1753–1758.